Electronic Supplementary Material (ESI) for Energy & Environmental Science.
This journal is © The Royal Society of Chemistry 2023

Supplementary Materials

A conformally bonded molecular interface retarded iodine migration for durable perovskite solar cells

Ligang Yuan,[1,†] Weiya Zhu,[1,†] Yiheng Zhang,[1] Yuan Li,[1,*] Christopher C. S. Chan,[2] Minchao Qin,[3] Jianhang Qiu,[4] Kaicheng Zhang,[5] Jiaxing Huang,[1] Jiarong Wang,[1] Huiming Luo,[1] Zheng Zhang,[1] Ruipeng Chen,[1] Weixuan Liang,[1] Qi Wei,[1] Kam Sing Wong,[2] Xinhui Lu,[3] Ning Li,[1,*] Christoph J. Brabec,[5, 6] Liming Ding,[7] Keyou Yan[1,*]

[1] School of Environment and Energy, State Key Laboratory of Luminescent Materials and Devices, Institute of Polymer Optoelectronic Materials and Devices, Guangdong Provincial Key Laboratory of Solid Wastes Pollution Control and Recycling, Guangdong Provincial Key Laboratory of Luminescence from Molecular Aggregates, AIE Institute, South China University of Technology, Guangzhou 510000, P. R. China

[2] Department of Physics and William Mong Institute of Nano Science and Technology, The Hong Kong University of Science and Technology, Clearwater Bay, Hong Kong, P. R. China

[3] Department of Physics, The Chinese University of Hong Kong, Shatin 999077, Hong Kong, P. R. China

[4] Shenyang National Laboratory for Materials Science, Institute of Metal Research, Chinese Academy of Sciences, Shenyang, 110016, China

[5] Institute of Materials for Electronics and Energy Technology (i-MEET) Friedrich-Alexander-University Erlangen-Nuremberg Martensstraße 7, Erlangen 91058, Germany

[6] Helmholtz-Institute Erlangen-Nürnberg for Renewable Energy (HI ERN), Forschungszentrum Jülich (FZJ), Erlangen 91058, Germany

[7] Center for Excellence in Nanoscience (CAS), Key Laboratory of Nanosystem and Hierarchical Fabrication (CAS), National Center for Nanoscience and Technology, Beijing 100190 P. R. China

[†] These two authors contributed equally to this work.

*Corresponding author: celiy@scut.edu.cn, ningli2022@scut.edu.cn, kyyan@scut.edu.cn

Materials and Methods

Materials: Methylammonium bromide (MABr, 99.5%), Methylammonium chloride (MACl, 99.5%), Lead iodide (PbI_2, 99.99%), lithium bistrifluoromethane-sulfonimidate (LiTFSI, 99.95%) and 4-tert-butylpyridine (tBP) were purchased from Xi'an polymer light technology Corp. Formamidinium iodide (FAI) and Guanidinium iodide (GAI) were purchased from Greatcell Solar. Ltd. Spiro-OMeTAD (99.86%) purchased from Advanced Election Technology Co., Ltd. The SnO_2 colloid precursor (tin(IV) oxide, 15% in H_2O colloidal dispersion) were acquired from Alfa Aesar.

Isopropanol (IPA, 99.5%), *N,N*-dimethylformamide (DMF, anhydrous, 99.8%), dimethyl sulfoxide (DMSO, anhydrous, 99.8%), chlorobenzene (CB, anhydrous, 99.8%) and acetonitrile (anhydrous, 99.9%) were acquired from Sigma-Aldrich and used as received without further purification. Commercially available reagents and chemicals were purchased from Suzhou Nakai Technology or Energy chemical and used without further purification.

Synthesis for dopant-free HTMs

Synthesis of TPAOMe-BT-Br

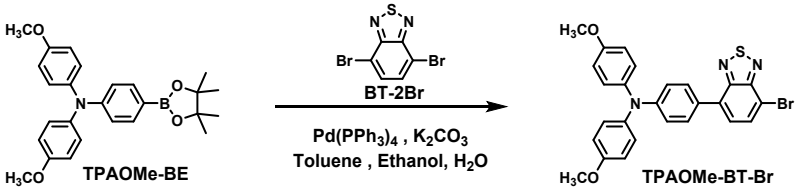

Scheme S1. Synthetic routes of **TPAOMe-BT-Br**.

TPAOMe-BE (3.448 g, 8.00 mmol, purchased from Suzhou Nakai Technology), **BT-2Br** (3.516 g, 12.00 mmol), $Pd(PPh_3)_4$ (30 mg, 0.026 mmol), potassium carbonate (K_2CO_3) aqueous solution (2 mol/L, 20 mL), ethanol (20 mL) and toluene (50 mL) were mixed and stirred under nitrogen atmosphere, and then heated to 100 °C and soaked for 12 h. After the reaction was completed, the mixture was cooled to room temperature and extracted three times with dichloromethane. The crude product was purified by column chromatography (silica gel, petroleum ether/dichloromethane, v/v, 3:1) to afford **TPAOMe-BT-Br** as a red solid compound (3.774 g, 91.0%). **^{1}H NMR (400 MHz, $CDCl_3$) δ 7.88 (d, J = 7.6 Hz, 1H), 7.75 (d, J = 8.5 Hz, 2H), 7.51 (d, J = 7.6 Hz, 1H), 7.13 (d, J = 7.3 Hz, 4H), 7.03 (d, J = 7.5 Hz, 2H), 6.87 (d, J = 8.9 Hz, 4H), 3.81 (s, 6H).**

Synthesis of L1

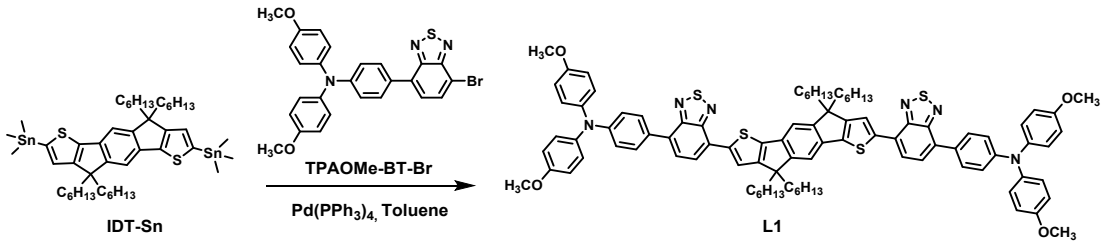

Scheme S2. Synthetic routes of **L1**.

TPAOMe-BT-Br (0.319 g, 0.62 mmol), **IDT-Sn** (0.260 g, 0.28 mmol), $Pd(PPh_3)_4$ (0.013 g, 0.011 mmol) and toluene (15 mL) were mixed and stirred under nitrogen atmosphere, and then heated to 110 °C and soaked for 4 h. After the reaction was completed, the mixture was cooled to room temperature and extracted three times with dichloromethane. The crude product was purified by column chromatography (silica gel, petroleum ether/dichloromethane, v/v, 2:1) to afford **L1** as a black solid compound (0.354 g, 85.5%). **^{1}H NMR (400 MHz, $CDCl_3$) δ 8.06 (s, 2H), 7.97 (d, J = 7.5 Hz, 2H), 7.85 (d, J = 8.6 Hz, 4H), 7.70 (d, J = 7.6 Hz, 2H), 7.39 (s, 2H), 7.15 (d, J = 8.7 Hz, 8H), 7.07 (d, J = 8.5 Hz, 4H), 6.88 (d, J = 8.8 Hz, 8H), 3.82 (s, 12H), 2.14 – 2.06 (m, 4H), 1.96 (t, J = 10.2 Hz, 4H), 1.13 (s, 24H), 0.98 (s, 4H), 0.90 (s, 4H), 0.77 (t, J = 6.6 Hz, 12H). ^{13}C NMR (126 MHz, $CDCl_3$) δ 156.20, 129.70, 127.07, 119.80, 114.79, 113.42, 55.54, 54.23, 39.30, 31.63, 29.78, 24.26, 22.61, 14.05.**

Synthesis of L2

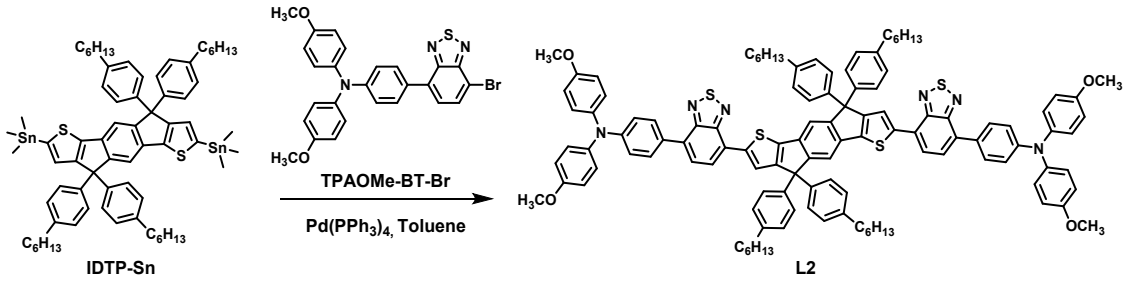

Scheme S3. Synthetic routes of **L2**.

TPAOMe-BT-Br (0.259 g, 0.499 mmol), **IDTP-Sn** (0.280 g, 0.227 mmol, purchased from Suzhou Nakai Technology), $Pd(PPh_3)_4$ (0.010 g, 0.009 mmol) and toluene (15 mL) were mixed and stirred under nitrogen atmosphere, and then heated to 110 °C

and soaked for 4 h. After the reaction was completed, the mixture was cooled to room temperature and extracted three times with dichloromethane. The crude product was purified by column chromatography (silica gel, petroleum ether/dichloromethane, v/v, 2:1) to afford **L2** as a black solid compound (0.366 g, 90.5%). **^{1}H NMR (400 MHz, $CDCl_3$) δ 8.01 (s, 2H), 7.95 – 7.71 (m, 6H), 7.53 (s, 6H), 7.28 (s, 2H), 7.26 – 7.17 (m, 4H), 7.10 (d, J = 8.1 Hz, 14H), 6.88 (s, 12H), 3.82 (s, 12H), 2.60 – 2.54 (m, 8H), 1.59 (p, J = 7.6 Hz, 8H), 1.34 (d, J = 7.6 Hz, 6H), 1.28 (d, J = 14.2 Hz, 18H), 0.86 (t, J = 6.5 Hz, 12H). ^{13}C NMR (126 MHz, $CDCl_3$) δ 141.91, 141.53, 128.42, 128.01, 55.51, 35.61, 31.74, 31.37, 29.18, 22.61, 14.12.**

Synthesis of L3

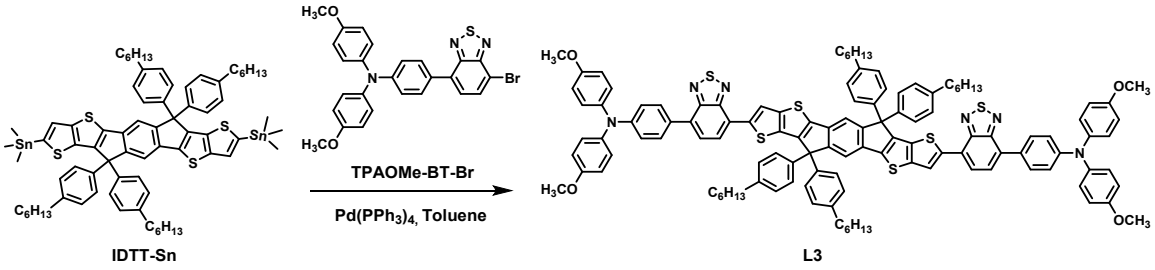

Scheme S4. Synthetic routes of **L3**.

TPAOMe-BT-Br (0.241 g, 0.466 mmol), **IDTT-Sn** (0.285 g, 0.211 mmol, purchased from Suzhou Nakai Technology), $Pd(PPh_3)_4$ (0.010 g, 0.009 mmol) and toluene (15 mL) were mixed and stirred under nitrogen atmosphere, and then heated to 110 °C and soaked for 4 h. After the reaction was completed, the mixture was cooled to room temperature and extracted three times with dichloromethane. The crude product was purified by column chromatography (silica gel, petroleum ether/dichloromethane, v/v, 2:1) to afford **L3** as a black solid compound (0.336 g, 83.8%). **^{1}H NMR (400 MHz, $CDCl_3$) δ 8.54 (s, 2H), 8.09 – 7.79 (m, 6H), 7.56 (s, 6H), 7.28 (s, 2H), 7.28 – 7.27 (m, 2H), 7.25 – 7.10 (m, 12H), 7.04 (s, 8H), 6.92 (s, 10H), 3.87 (s, 12H), 2.61 – 2.55 (m, 8H), 1.62 (d, J = 14.5 Hz, 8H), 1.39 – 1.27 (m, 24H), 0.86 (s, 12H). ^{13}C NMR (126 MHz, $CDCl_3$) δ 141.85, 140.19, 128.55, 128.13, 55.52, 35.63, 31.72, 31.28, 29.20, 22.61, 14.10.**

Fabrication of devices: ITO glass substrates (Advanced Election Technology Co., Ltd.) were cleaned sequentially by sonication in detergent, deionized water, acetone, ethanol and isopropanol, twice for each liquid and 15 min for each time, followed by ultraviolet-ozone treatment for 30 min. The SnO_2 electron transport layer was coated onto the ITO substrate with diluted SnO_2 nanoparticles solution (2.67%) in ambient air, and then annealed at 150 °C for 30 min. After being cooled to room temperature, the substrate was treated with UV-ozone for 30 min before spin-coating of perovskite solution. The perovskite layer was deposited by a two-step spin coating method; first, 360 mg PbI_2 and 10.2 mg CsI in 600 μL dissolved in mixed solvent (DMF:DMSO (v/v=95:5)) followed by stirring at 70 °C for 4 h, then the PbI_2 solution was spin coated onto the SnO_2 ETL at 2500 rpm for 50 s, during this process, the mixture organic amino solution of FAI:MABr:MACl:GAI (60 mg:6 mg:6 mg:4 mg in 1 mL isopropanol) was adding before the end of 30 s, and then the perovskite film was annealed in at 150 °C for 11 min. For the doped spiro-OMeTAD-based devices, 72.3 mg/mL spiro-OMeTAD with 28.8 μL tBP and 17.5 μL Li-TFSI (520 mg/mL in Acetonitrile) in CB was deposited by spin-coating at 4000 rpm for 30 s. For dopant-free HTM devices, different concentrations in CB solution with different speeds were spin coating on the perovskite film. Finally, MoO_3 blocking layer (6 nm) and metal electrode (80 nm) were eventually deposited by vacuum thermal evaporation (pressure < 2×10^{-4} Pa). The overlapping area between the cathode and anode defined a pixel size of 0.08 cm^{-2}.

HTMs characterizations:

^{1}H-NMR spectra were recorded by DRX-400 spectrometer (400 and 500 MHz ^{1}H-NMR frequency, Bruker Co., Ettlingen, Germany) in $CDCl_3$ at room temperature. ^{13}C NMR spectra were collected using the same instrument at 126 MHz. The mass spectra were recorded on MALDI-TOF/TOF 5800 system (AB SCIEX). Cyclic voltammetry (CV) tests were performed in CH_2Cl_2 solution with 0.1 M tetrabutylammonium hexafluorophosphate (Bu_4NPF_6) as the electrolyte at a scan rate of 50 mV/s, a

$Hg/HgCl_2$ (Saturated KCl solution) electrode as the reference electrode, a carbon-glass electrode as the working electrode, a Pt line electrode as the counter electrode and ferrocene/ferrocenium (Fc/Fc^+) as an internal reference on electrochemistry workstation (CHI660E, China). XPS results were acquired on a photoelectron spectrometer (ESCALAB 250Xi, Thermo Fisher Scientific). Thermogravimetric analysis (TGA) was performed on a thermogravimetric analyzer (TA Instruments) at a scan rate of 20 K/min in the nitrogen atmosphere. Differential scanning calorimetry (DSC) was recorded on a DSC201F2 differential scanning calorimeter under the protection of nitrogen at a heating rate of 10 K/min.

DFT calculation: The neutral and charged molecular geometries are optimized by the DFT method with the Lee-Yang-Parr (B3LYP) hybrid functional and 6-31G(d,p) basis set implemented in the Gaussian 09 package.

Film characterizations measurements:

The absorption spectrum of HTMs and perovskite films were tested using a Cary Series UV-Vis-NIR Spectrophotometer.

Contact angle measurements were conducted on ZJ-7000 with a drop of ultrapure water (0.002 mL). The photographs were taken 1 second after water dripping.

The perovskite film and HTMs surface morphology were characterized by atomic force microscope (AFM, Bruker, Santa Barbara, CA).

Fourier transform infrared spectra were obtained on a CCR-1 instrument (Thermo Nicolet). PbI_2 and L3 are the pure powders. The PbI_2/L3 sample was mixed PbI_2 solution and L3 solution directly, then the powder was dried at 80 °C for eight hours. For the ART FTIR measurements, the perovskite film covered L3 film by spin-coating 1mg/mL L3 CB solution with a speed of 3000 rpm 30s.

The top-view and cross-sectional SEM images of the samples were characterized using a high-resolution scanning electron microscope (Zeiss Merlin). An electron beam accelerated to 5 kV was used with an InLens detector.

Transmission electron microscope (TEM, JEOL JEM-2100 Plus) measurements were performed under 200 kV. We exfoliated the films from the substrates by floating technique with orthogonal solvent. The substrates with a structure of ITO/PEDOT:PSS/HTM prepared by spin-coating, then deionized water were employed to dissolve the bottom PEDOT:PSS film, leaving behind HTM film on the surface. The films were collected by copper grid for characterization.

The GIWAXS measurements were performed with a Xeuss 2.0 SAXS/WAXS laboratory beam line using a Cu X-ray source (8.05 keV, 1.54 Å) and a Pilatus3R 300K detector. The incidence angle was 0.2º.

Time resolved photoluminescence (TRPL) was performed on encapsulated films of glass substrate/perovskite/HTM. The samples were excited from the top surface with a 640 nm sub-100ps diode laser (Edinburgh Instruments EPL640). The PL was collected and diverted into a monochromator transmitting the peak PL wavelength and collected by a single photon counter to carry out time correlated single photon counting with a Becker and Hickl system. The time resolution is <500 ps.

Transient absorption spectroscopy was carried out on encapsulated pure HTM films to minimize photooxidation and environmental degradation during the measurement. A Ti:Sapphire regenerative laser amplifier (Coherent Legend) provided 800 nm fundamental pulses with pulse width of 100 fs at 1 kHz. Excitation pump pulses at 400 nm was generated by splitting the fundamental pulse into an optical parametric amplifier (Opera Solo). The probe beam is set on a mechanical delay stage and focused onto a YAG crystal to generate a stable supercontinuum for broadband absorption probe. The pump and probe beams are spatially overlapped on the sample surface and the transmission is collected by a spectrometer (Acton SpectraPro 275) equipped with a line array CCD.

Device characterizations measurements:

J–V characteristics of photovoltaic cells were taken using a Keithley 2400 source measurement unit under a simulated AM 1.5G spectrum. With a SS-F5-3A solar simulator (Enli Technology CO., Ltd.), the light intensity was calibrated by standard KG3 reference silicon solar cells.

The Mott-Schottky plot measurements were measured by an IM6 electrochemical workstation (Zahner Zennium, Germany) at room temperature in ambient conditions. IPCE measurements also were performed on a Zahner system, using a TLS03 light source (300 HZ, 100 counts) at mixed mode.

Mobility and trap state density measurements:

Hole-only devices (ITO/PEDOT:PSS/HTL/MoO_x/Ag) were fabricated to calculate the hole mobility. The dark *J-V* characteristics of the hole-only devices were measured by a Keithley 2400 source.

The mobility of L-series HTLs is extracted by fitting the *J-V* curves by the Mott-Gurney equation of $J = 9\varepsilon_r\varepsilon_0 V^2/(8L^3)$.

The trap state density of perovskite film was determined by the trap-filled limit voltage using the equation of $n_t = 2\varepsilon\varepsilon_0 V_{TFL}/(qL^2)$ with a structure of ITO/PEDOT:PSS/perovskite/HTL/MoO_x/Ag.

Stability measurements: For the long-term storage stability, the unencapsulated PSCs with Ag top electrode were stored at argon filled glovebox under dark condition.

For thermal stability measurement (85°C), Ag electrode was replaced by Au and the PSCs were heated on a hotplate under dark condition, and the temperature was cooled down to room temperature before 30 min of PCE test.

For photo-thermal stability measurement (MPP & 85°C), The illumination was provided by white light-emitting diode lamp in a Lifetime Test equipment (Guangzhou Crysco Equipment Co.Ltd, P3000), and the radiation intensity is adjusted according the J_{SC}, which is equal to the J_{SC} under solar simulator. The temperature of PSCs was provided an electric resistance heater and control by a temperature controller, and the temperature error is 0.2°C. In this study, our temperature was set to 85°C in argon filled glovebox.

For the XRD and optical images teats for thermal aged perovskite film covered with HTMs, the prepared ITO/SnO_2/perovskite/HTM samples were heated on the hotplate with a temperature of 85°C in argon filled glovebox.

For the AFM and optical microscope image for thermal aged HTM measurements, the 15mg/mL HTMs were spin-coated on the SnO_2/ITO glass substrates and heated on the hotplate with a temperature of 100°C in nitrogen filled glovebox.

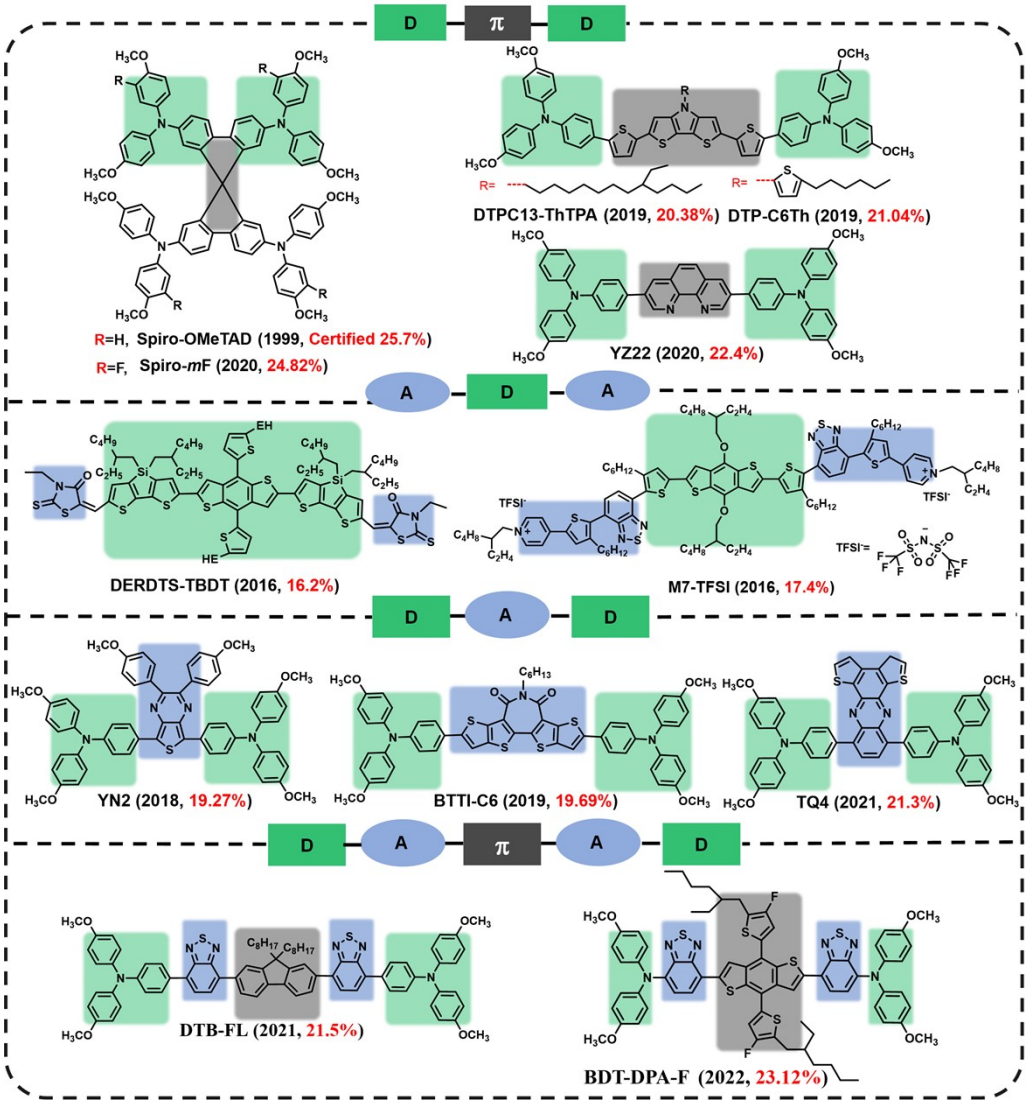

Fig. S1. Some established molecular structures of D-π-D, A-D-A and D-A-D HTMs for PSCs.[1-12]

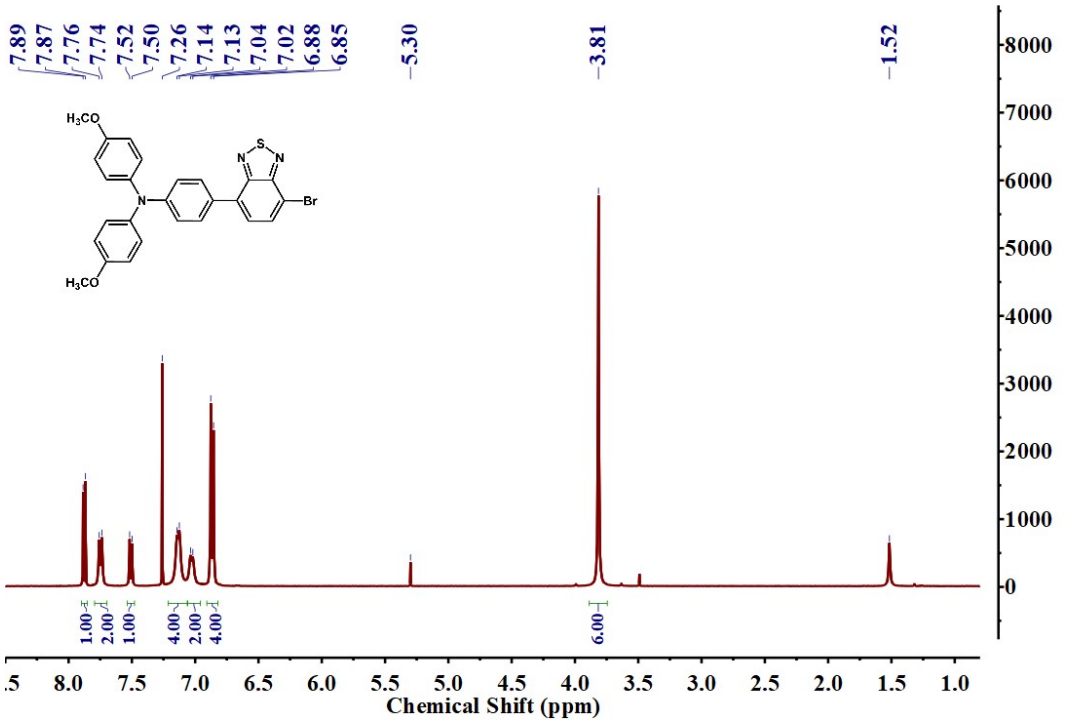

Fig. S2. **^{1}H NMR** spectrum of **TPAOMe-BT-Br**.

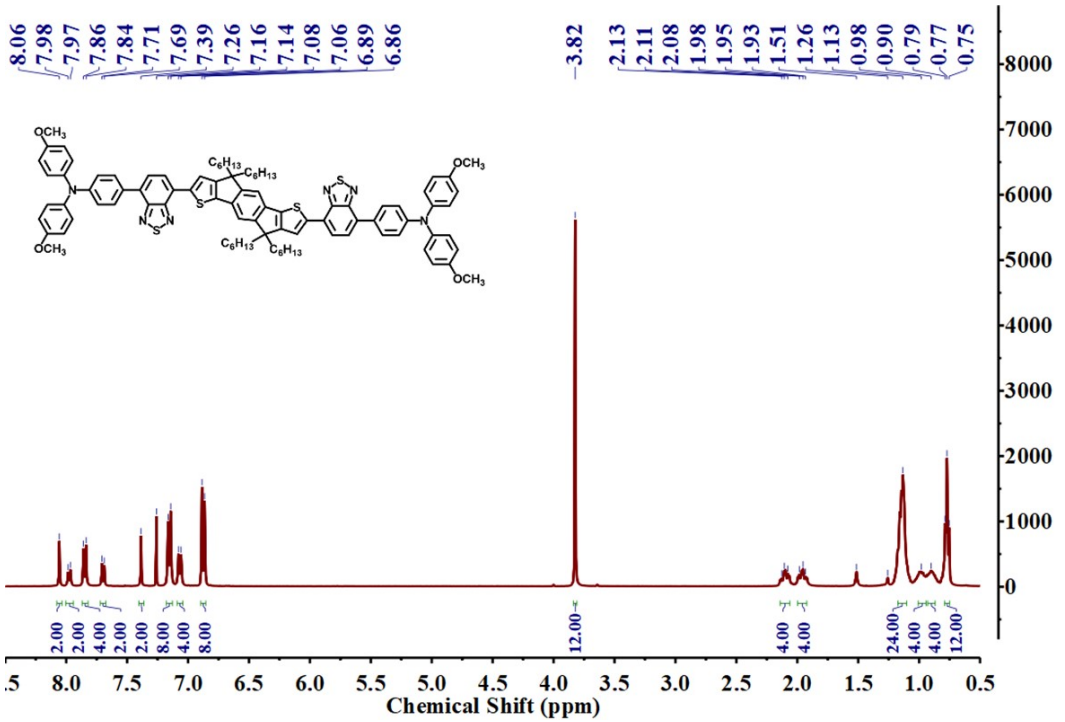

Fig. S3. **^{1}H NMR** spectrum of **L1**.

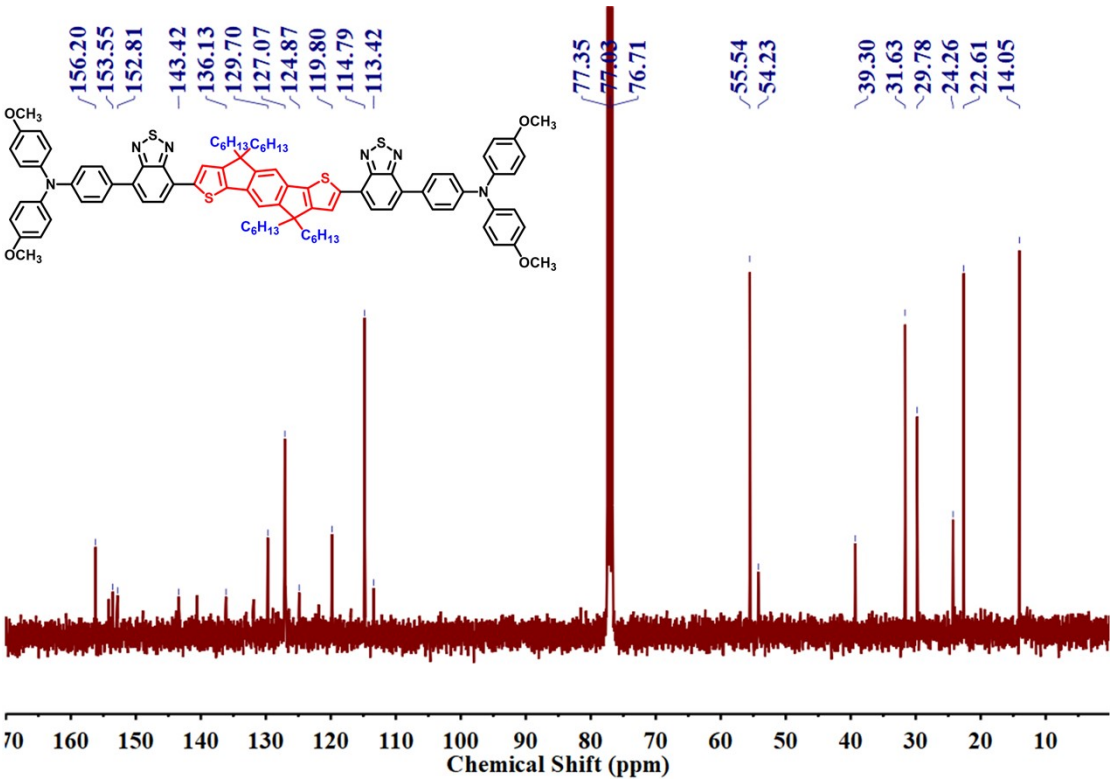

Fig. S4. **^{13}C NMR** spectrum **L1**.

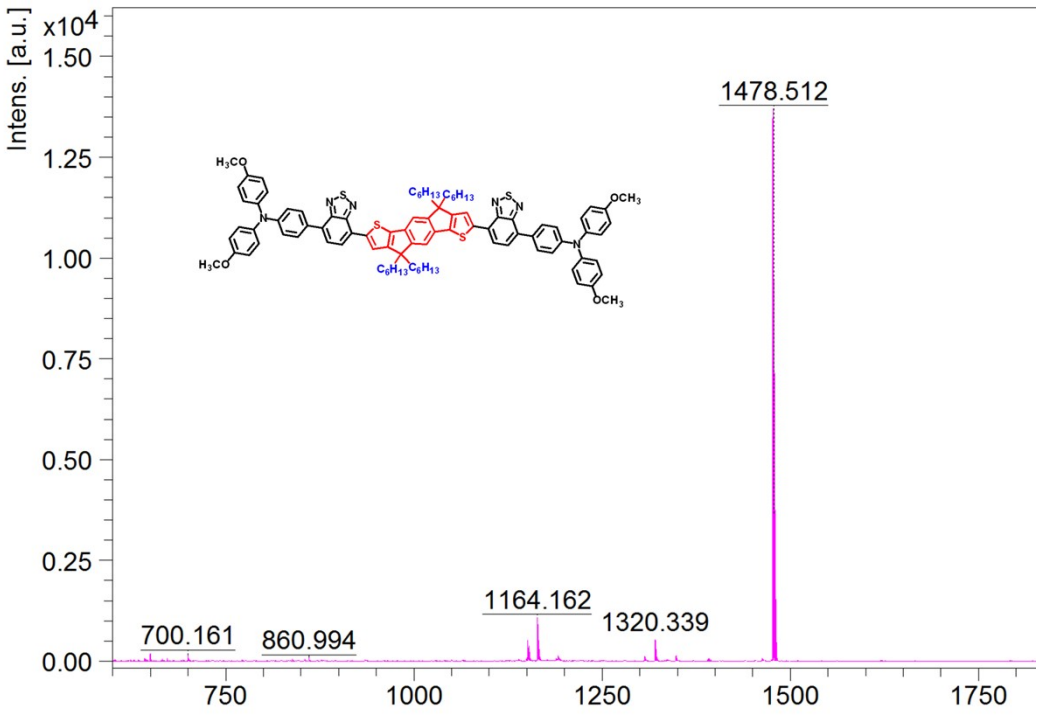

Fig. S5. MALDI-TOF-MS (m/z) spectrometry of **L1**: calcd. for $C_{92}H_{96}N_6O_4S_4$, 1478.06; found: 1478.516.

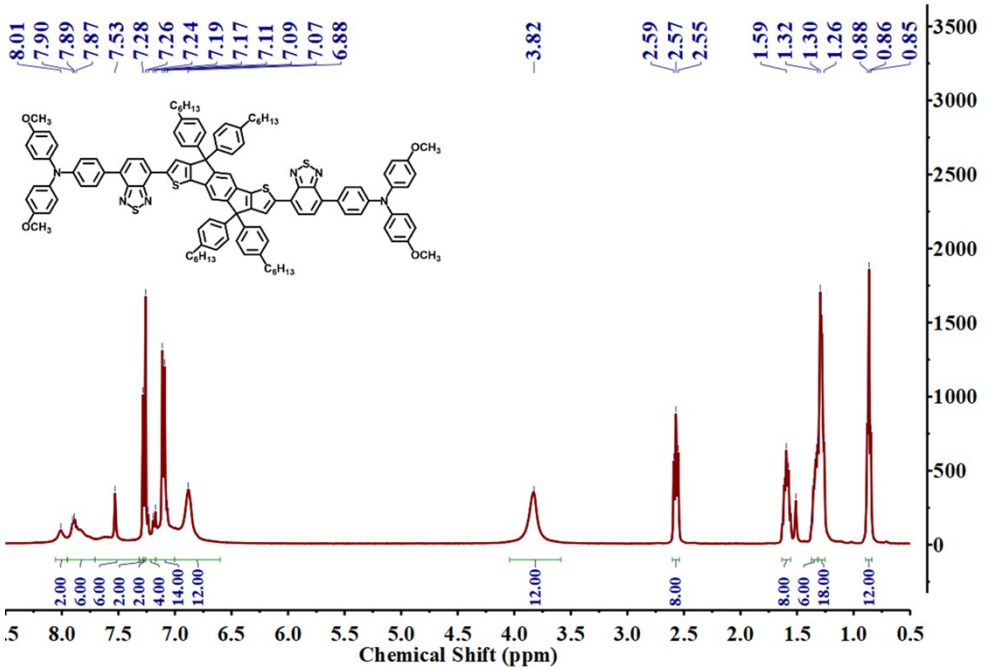

Fig. S6. ^{1}**H NMR** spectrum of **L2**.

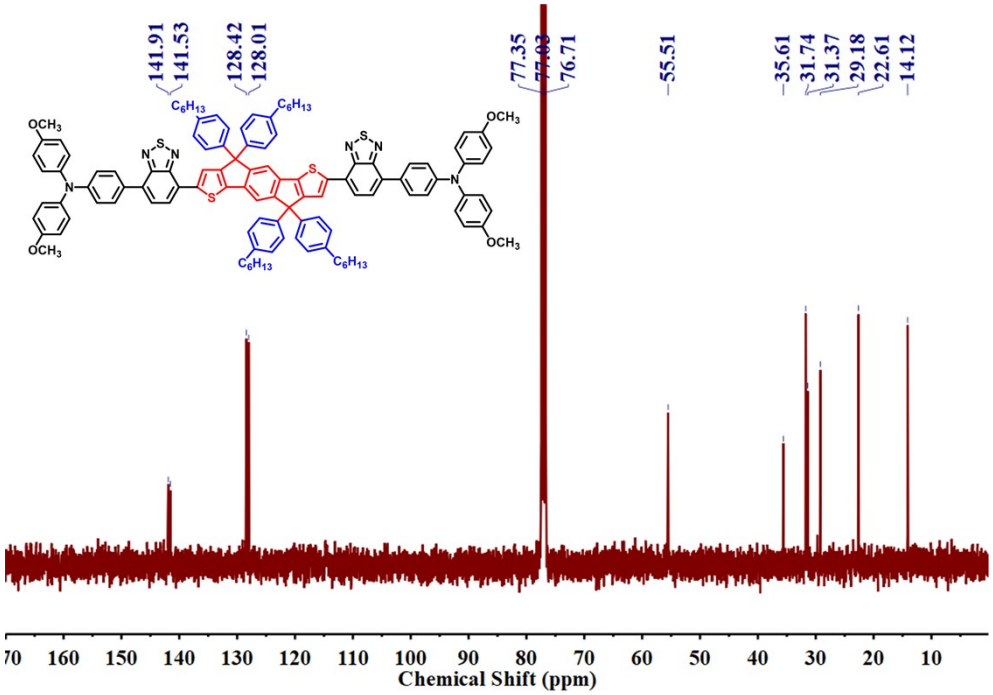

Fig. S7. ^{13}**C NMR** spectrum **L2**.

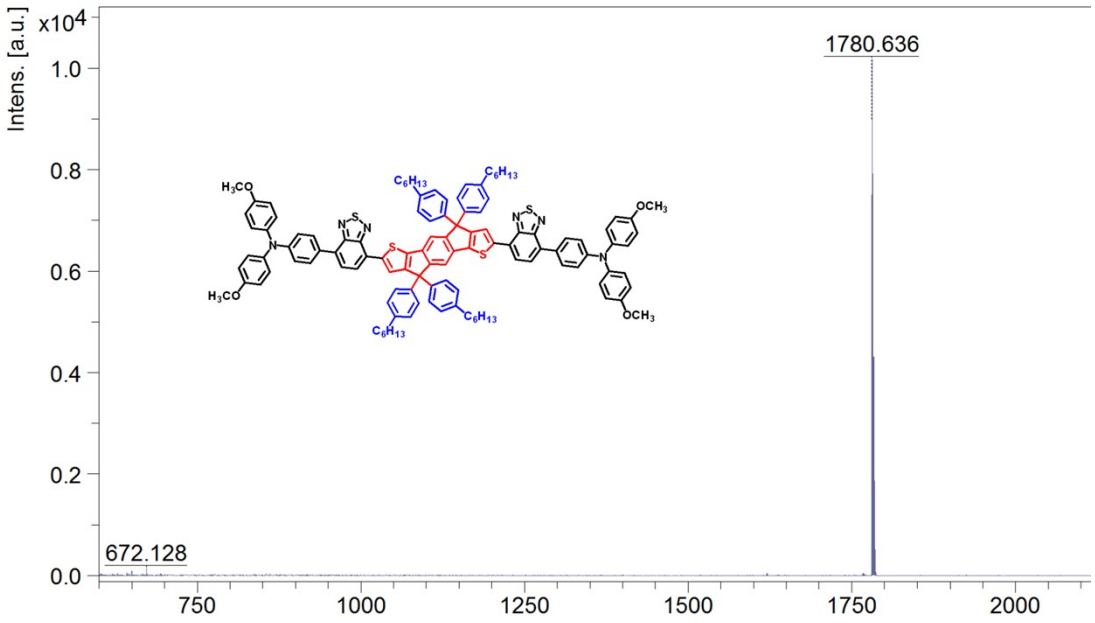

Fig. S8. MALDI-TOF-MS (m/z) spectrometry of **L2**: calcd. for $C_{116}H_{112}N_6O_4S_4$, 1782.45; found: 1780.636.

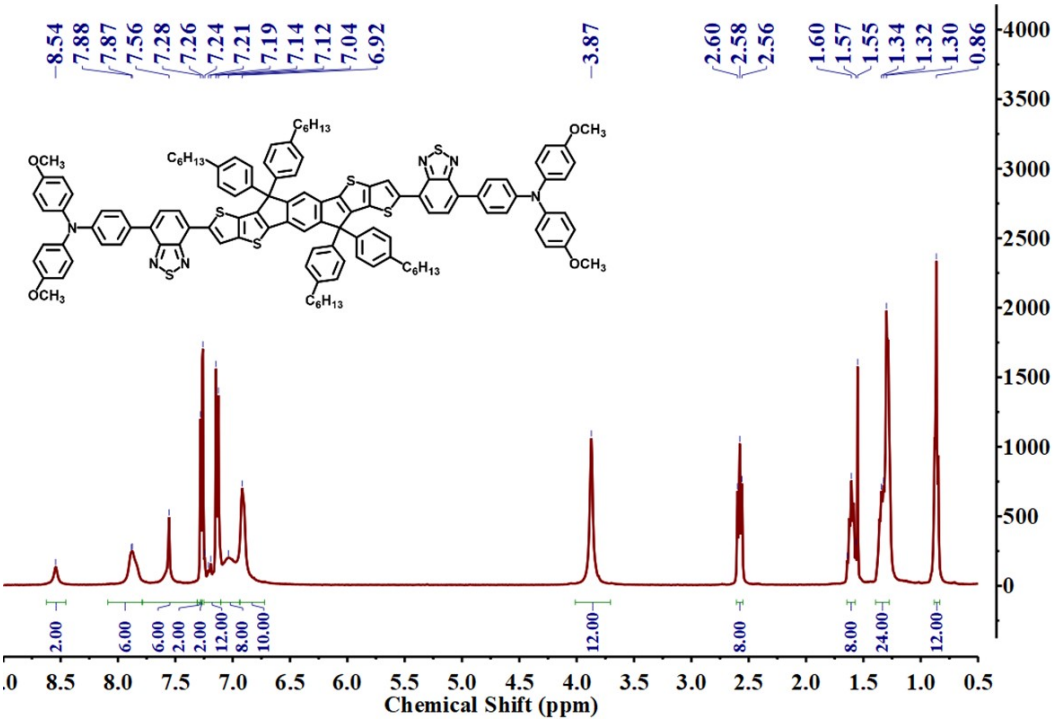

Fig. S9. ^{1}**H NMR** spectrum of **L3**.

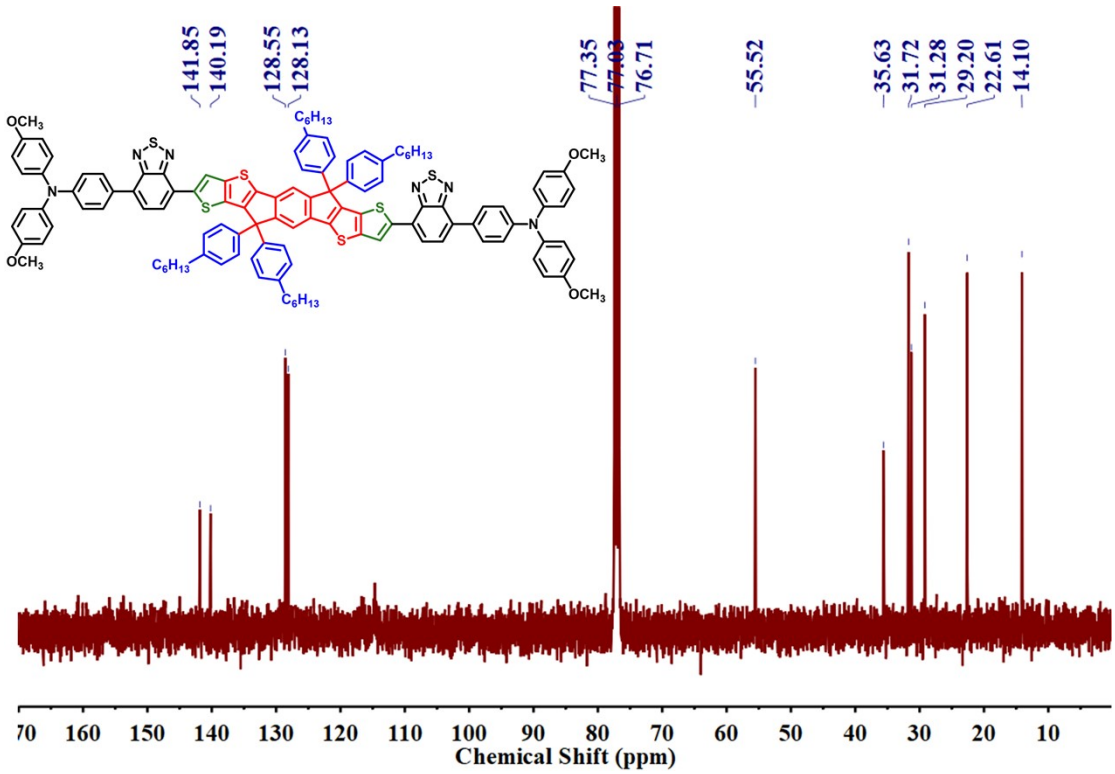

Fig. S10. ^{13}**C NMR** spectrum **L3**.

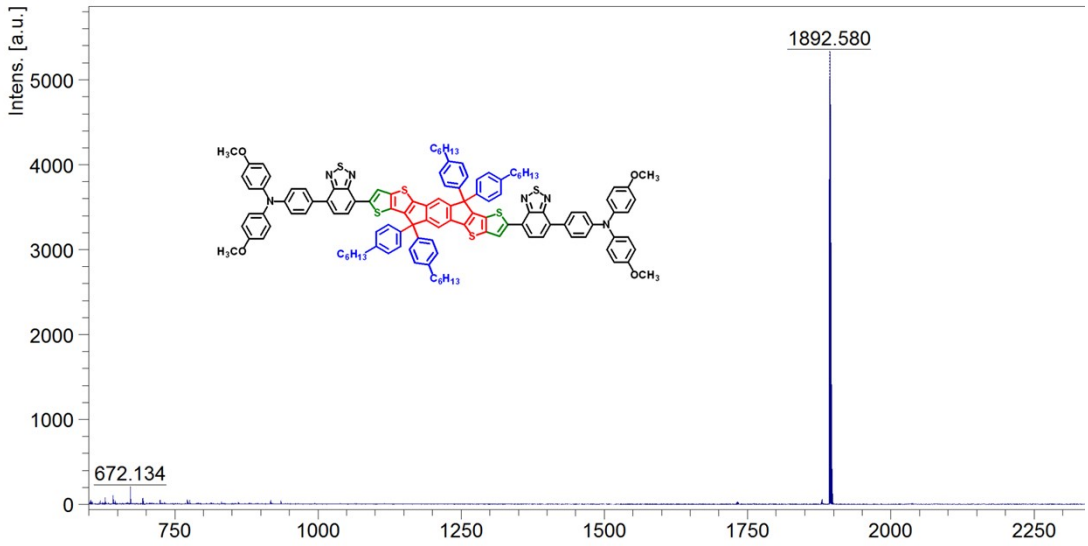

Fig. S11. MALDI-TOF-MS (m/z) spectrometry of **L3**: calcd. for $C_{120}H_{112}N_6O_4S_6$, 1894.61; found: 1892.580.

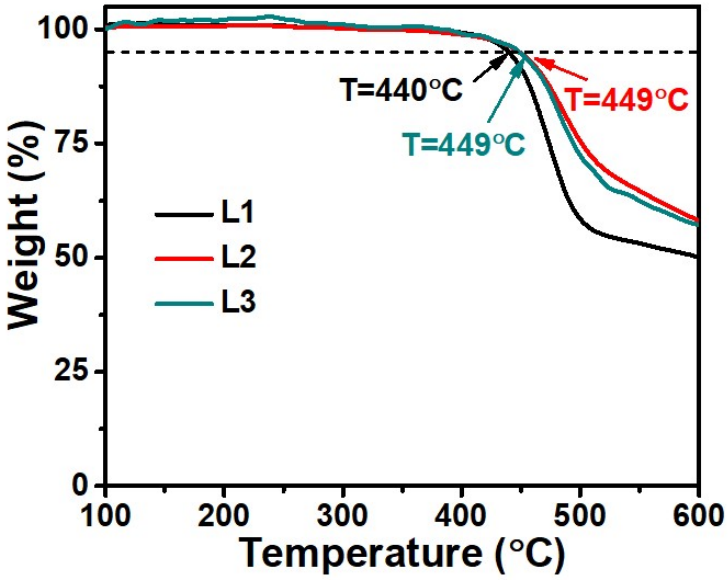

Fig. S12. TGA curves of **L1**, **L2**, and **L3** HTMs. Thermogravimetric analysis (TGA) was performed on a NETZSCH TG 209. Under nitrogen protection, the percentage of sample mass loss was collected at a heating rate of 10 °C/min, and the temperature corresponding to 5% sample mass loss was calculated.

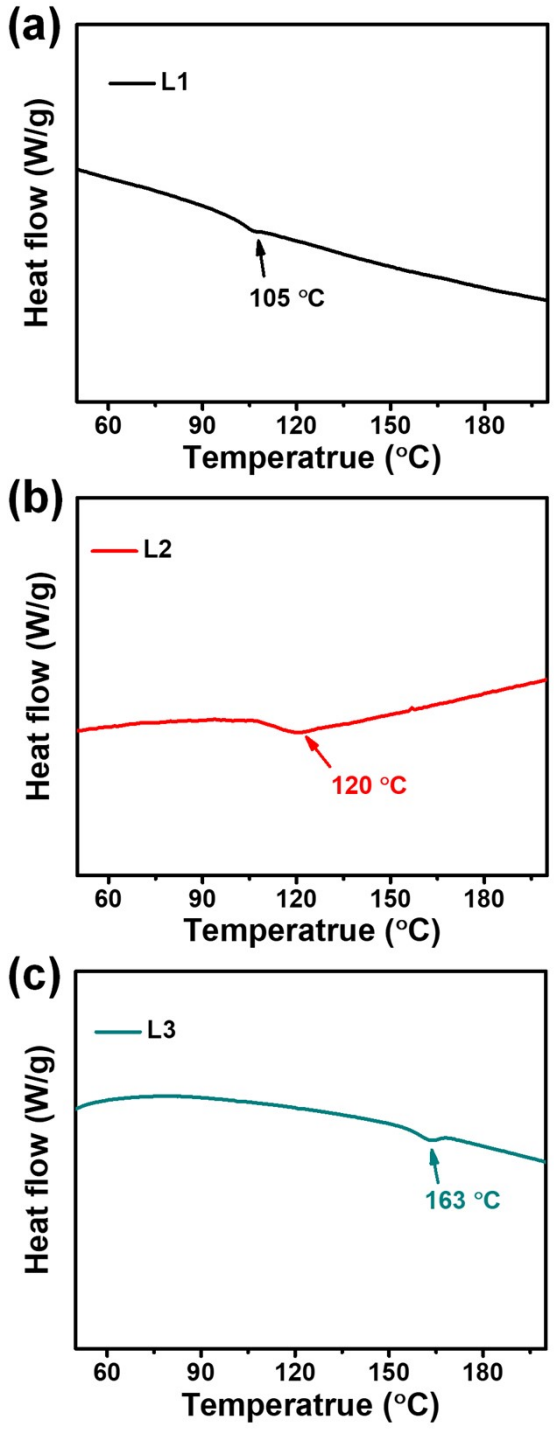

Fig. S13. Differential scanning calorimetry (DSC) curves of (a) **L1**, (b) **L2** and (c) **L3** HTMs. DSC was performed on a Netzsch DSC 200F3 under nitrogen at a heating rate of 10 °C/min to record the heat absorbed or released by the sample, and calculate the melting point of each material. The glass transition temperatures (T_g) of the three molecules are marked in the figure.

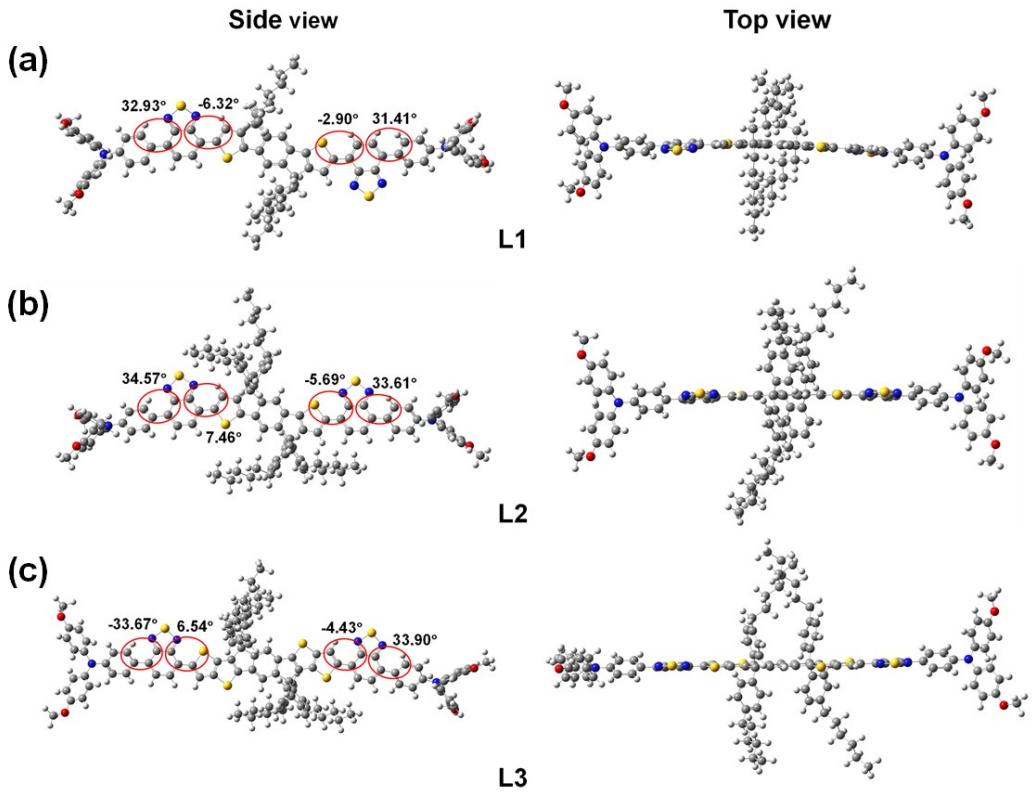

Fig. S14. DFT calculated optimized molecular conformations of **L1**, **L2** and **L3**, respectively. Compared with the **L2**, the torsion angle between the planes of the structural units in the **L3** is smaller, and the shape of **L3** is closer to the plane.

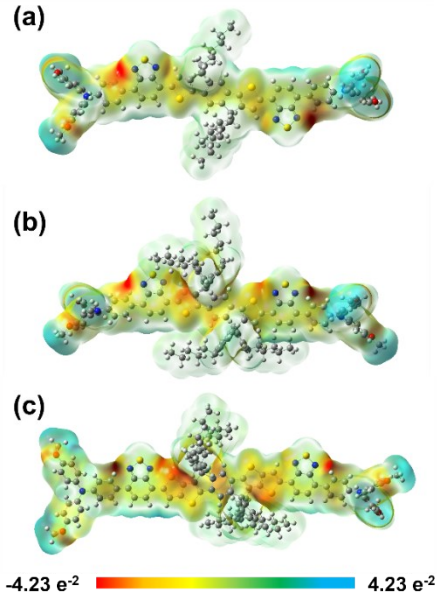

Fig. S15. Electrostatic surface (ESP) potential of (a) **L1**, (b) **L2**, and (c) **L3** molecules. The red and blue colors indicate negative and positive potentials, respectively.

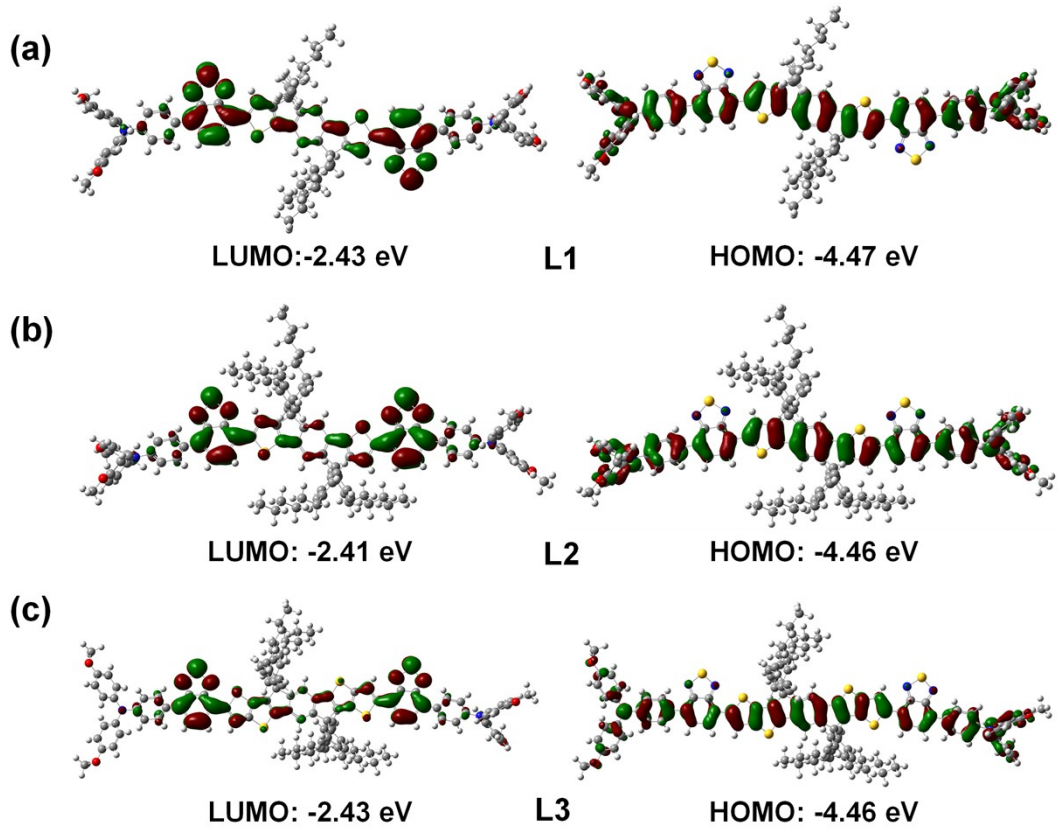

Fig. S16. DFT calculated molecular frontier orbitals of the LUMO and HOMO levels of (a) **L1**, (b) **L2**, and (c) **L3** molecules.

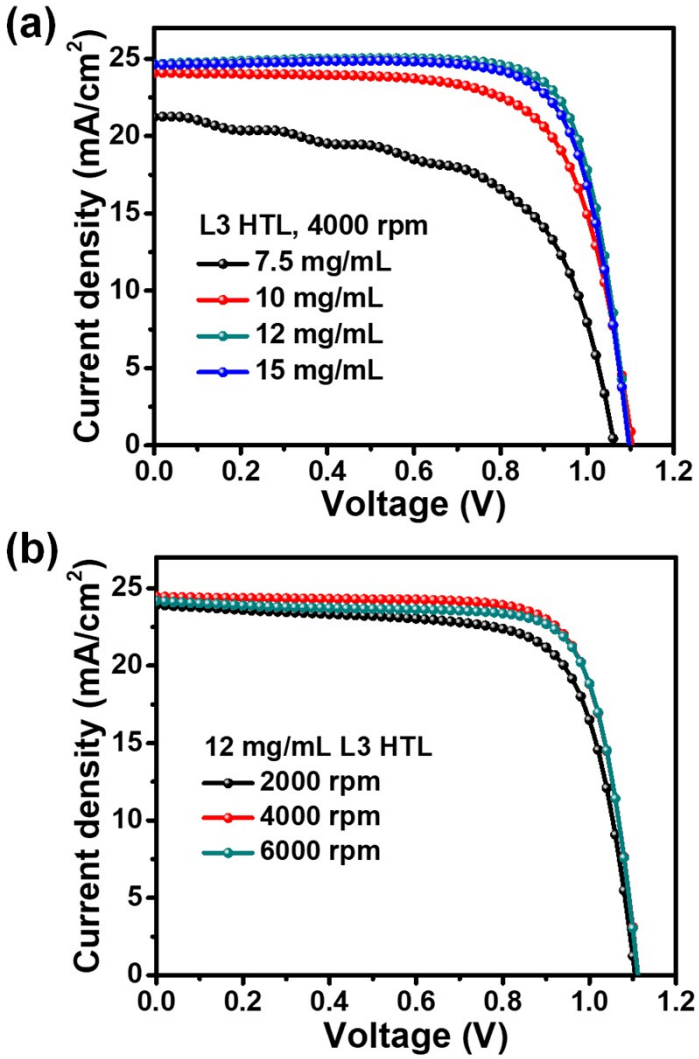

Fig. S17. *J-V* curves of PSCs. (a) different concentration of **L3**, (b) 12 mg/mL **L3** with different speed of spin-coating.

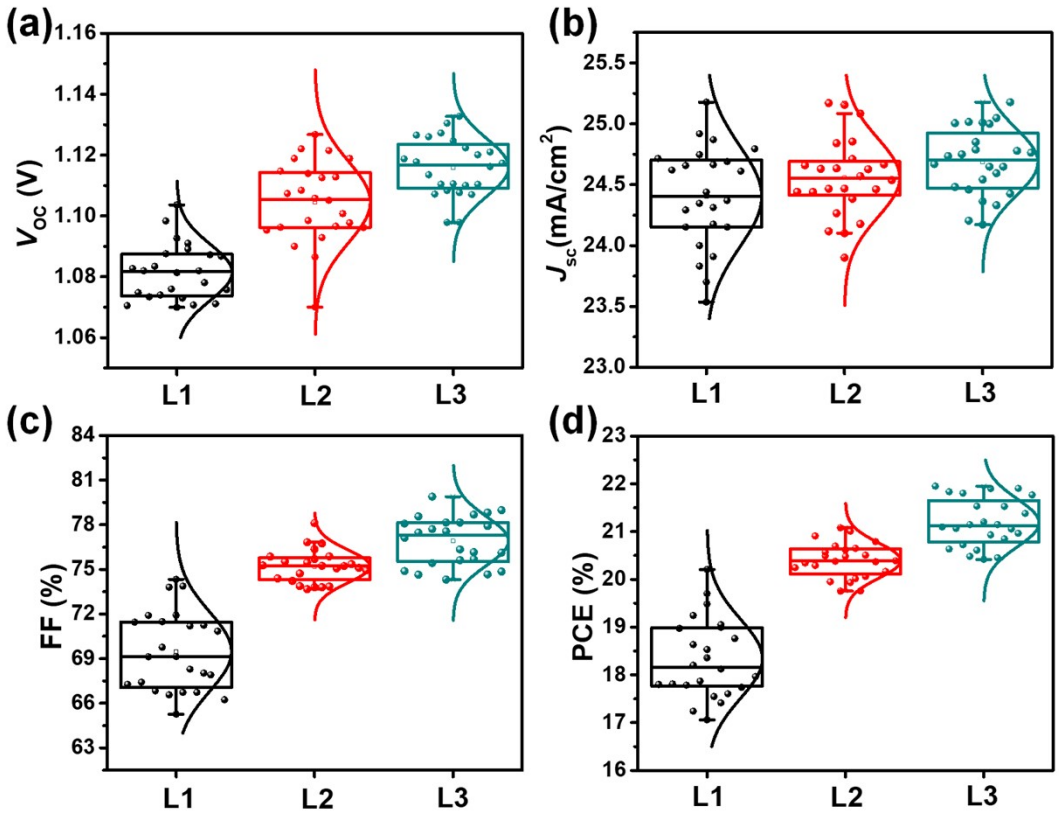

Fig. S18. Histogram of the PSCs with dopant-free HTMs of **L1**, **L2** and **L3**, analyzed from 24 cells. (a) V_{OC}, (b) J_{SC}, (c) FF, and (d) PCE.

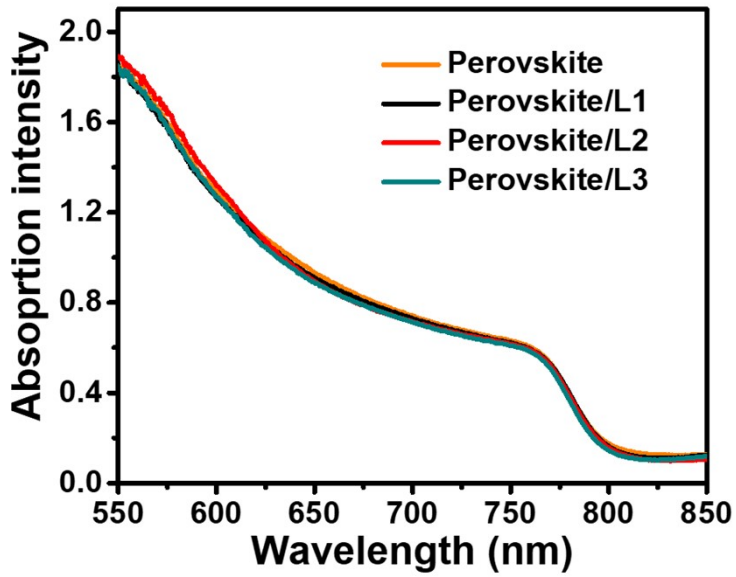

Fig. S19. The absorption spectra of perovskite and perovskite film cover with **L1**, **L2** and **L3** HTL, respectively.

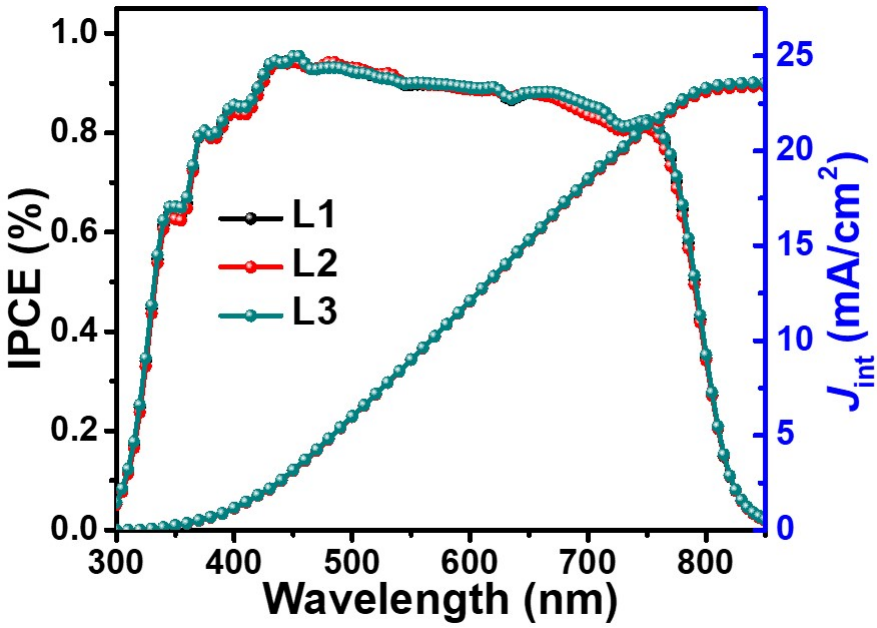

Fig. S20. IPCE curves and integrated J_{SC} of the best PSC with **L1**, **L2**, and **L3**, respectively.

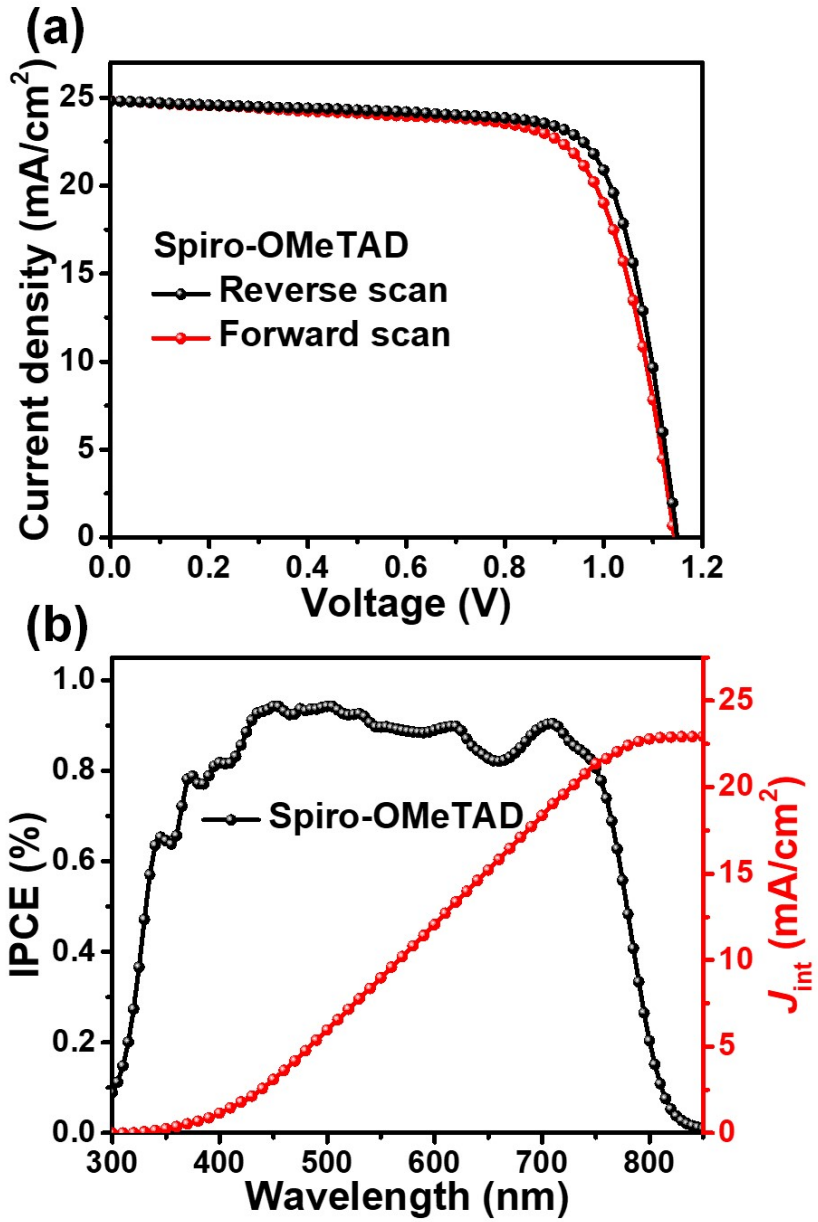

Fig. S21. (a) *J-V* curves and (b) IPCE spectra of PSC with doped **spiro-OMeTAD** HTL

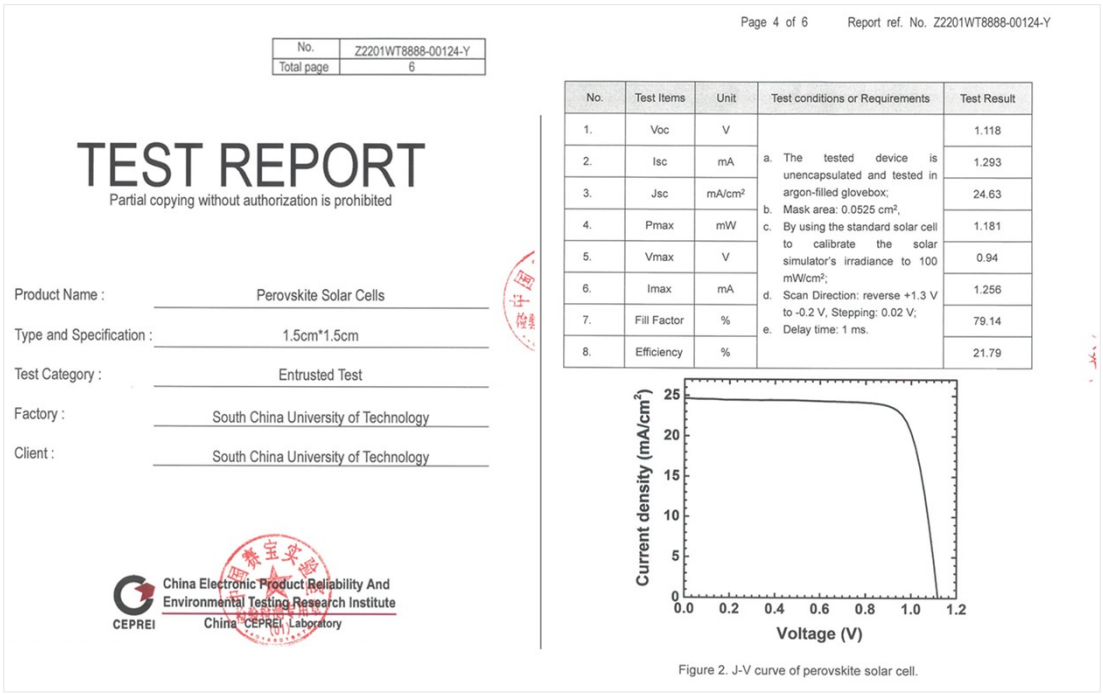

Fig. S22. The certified result of a perovskite solar cell measured by China CEPREI Laboratory. The device achieved V_{OC} of 1.12 V, a J_{SC} of 24.63 mA/cm^2 and an FF of 79.14% and a PCE of 21.79% with a mask area of 0.0525 cm^2.

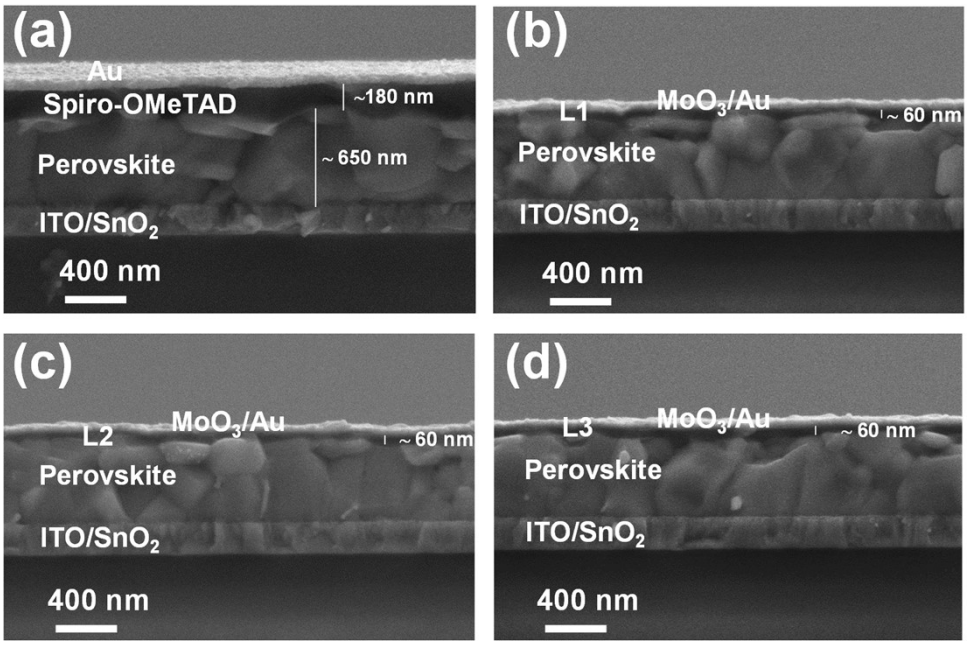

Fig. S23. Across-section SEM images of full PSCs. (a) PSC with doped **spiro-OMeTAD** HTM, (b) PSC with **L1** HTM, (c) PSC with **L2** HTM, and (d) PSC with **L3** HTM.

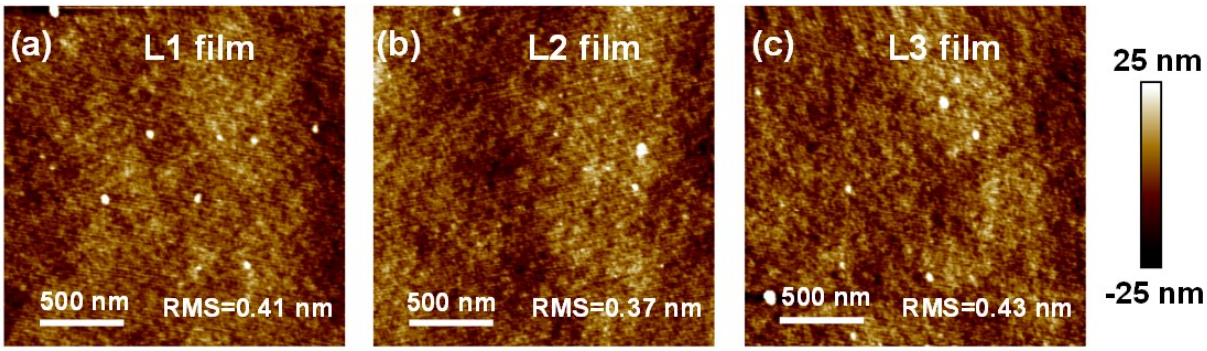

Fig. S24. AFM images of (a) **L1** film, (b) **L2** film and (c) **L3** film. All the HTM films were deposited on silicon wafer substrate.

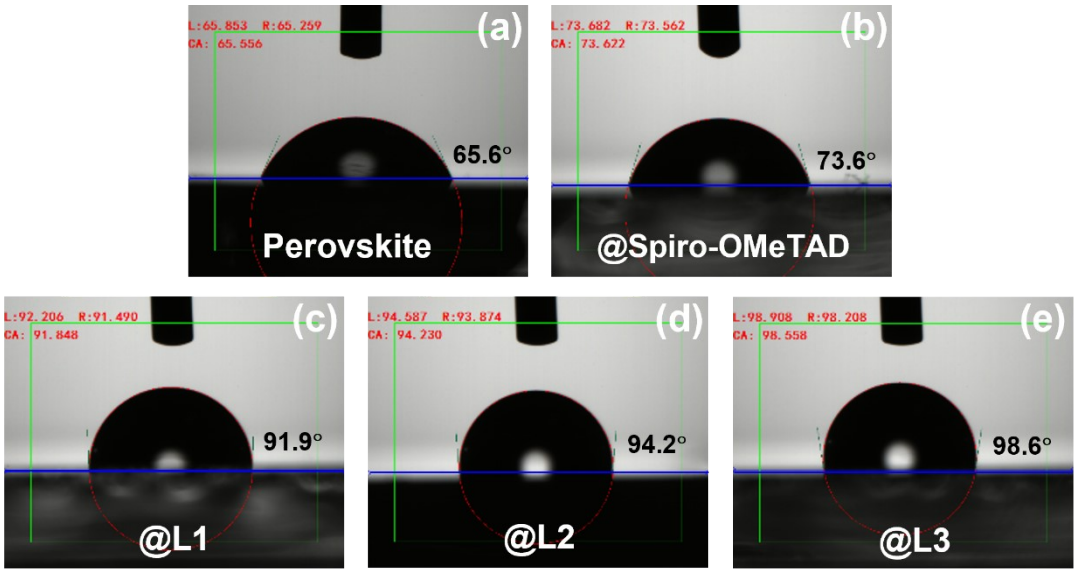

Fig. S25. The images of water contact angle of various surfaces: (a) perovskite film, (b) perovskite film with doped **spiro-OMeTAD** HTL (c) perovskite film with **L1** HTL, (d) perovskite film with **L2** HTL, and (e) perovskite film with **L3** HTL.

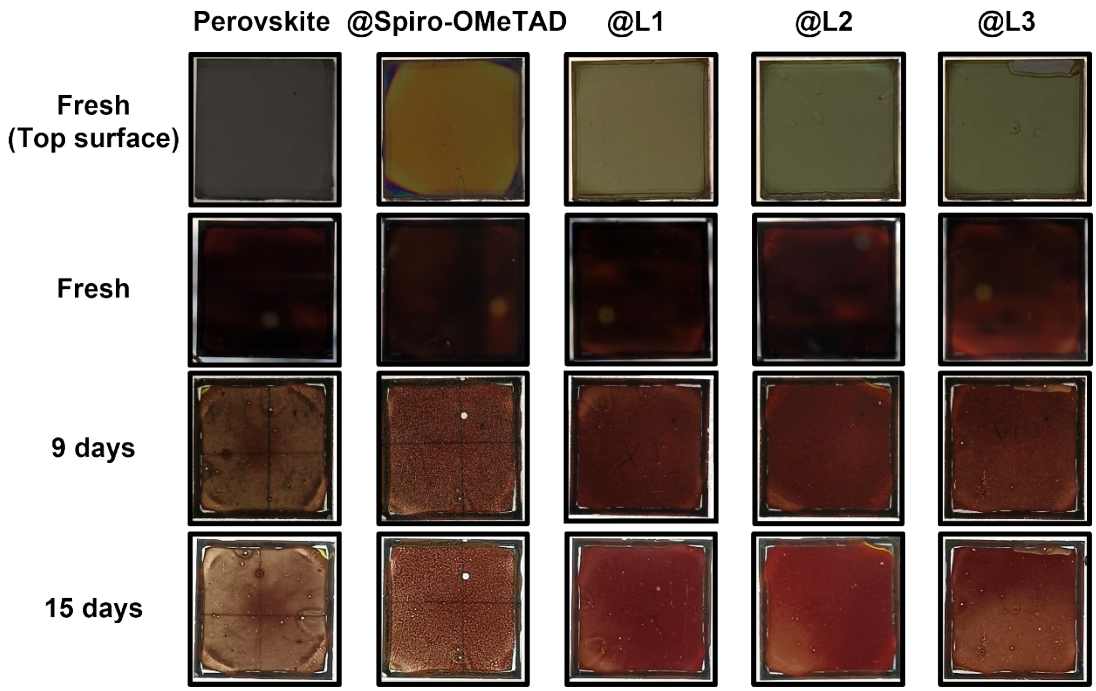

Fig. S26. The degradation images of the perovskite film with different HTL (glass/ITO/SnO_2/perovskite/HTM) under ambient atmosphere with RH=50-60%.

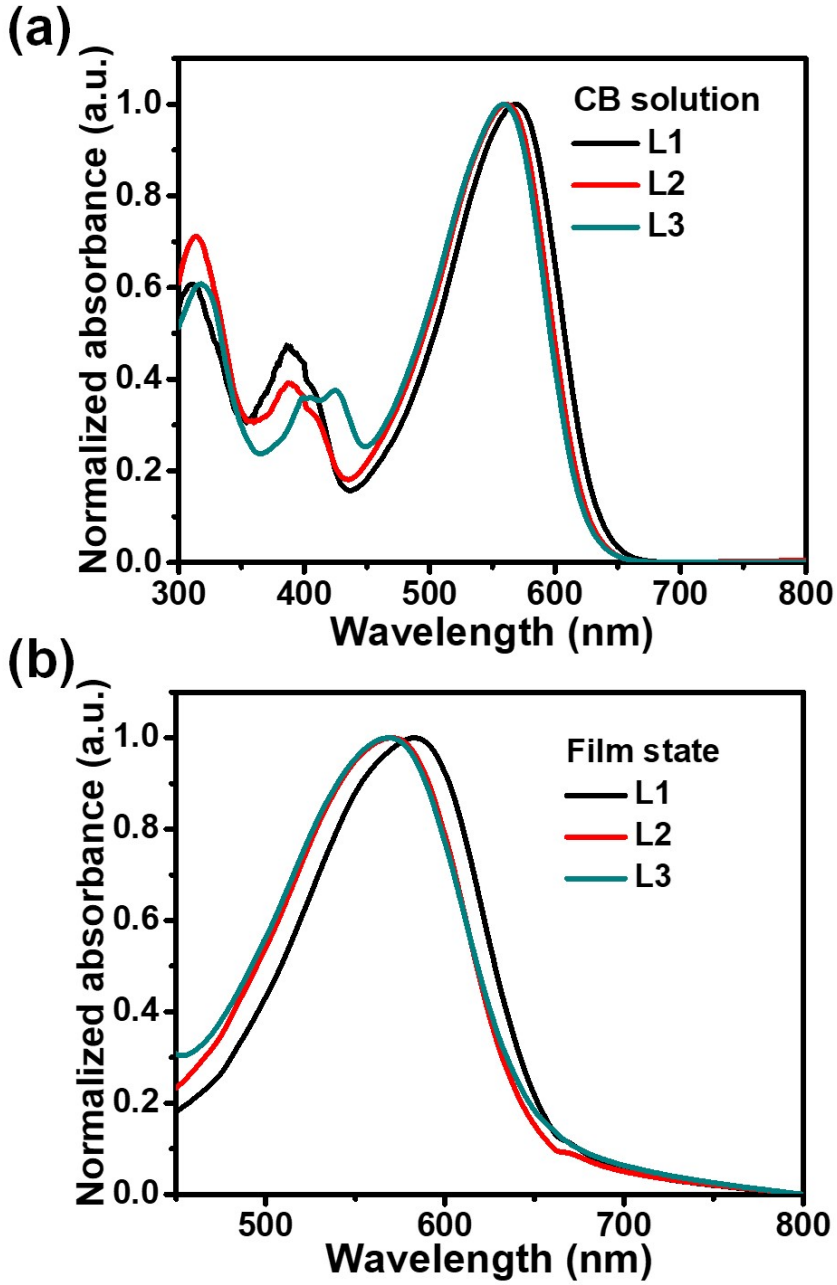

Fig. S27. Normalized UV-Vis absorption spectra of the HTMs in (a) CB solution and (b) film state.

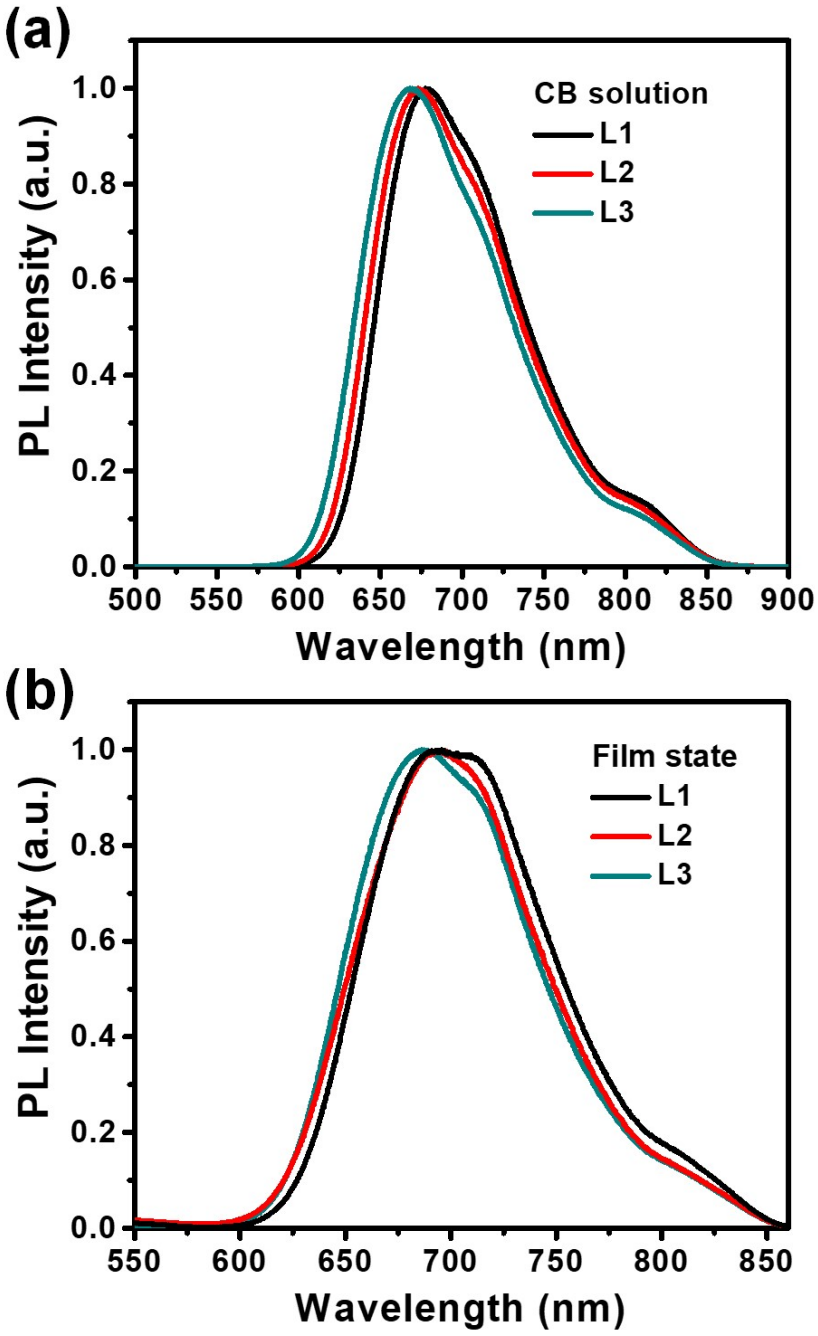

Fig. S28. Steady-state PL of **L1**, **L2** and **L3** HTMs. (a) solution state and (b) film state.

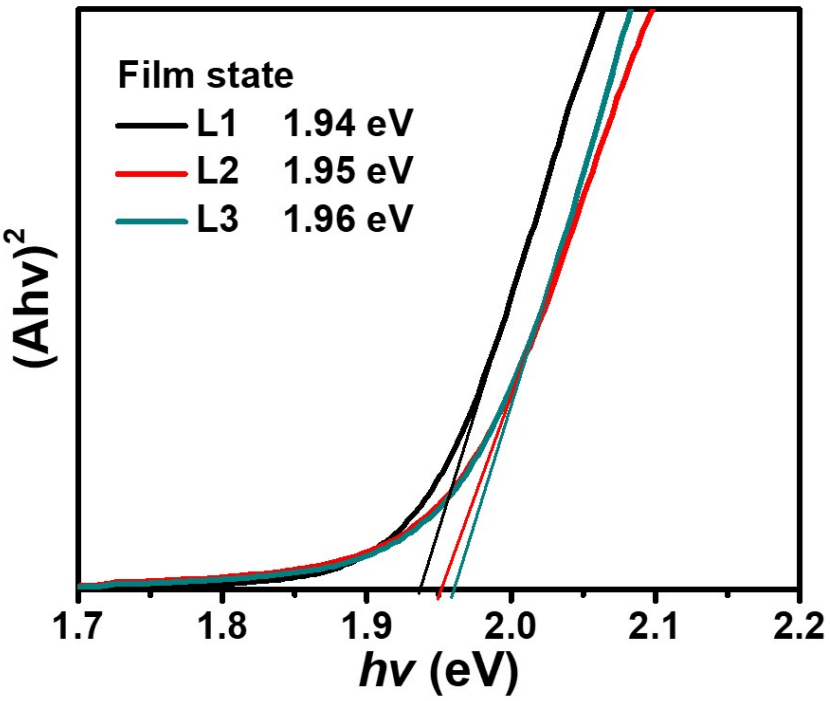

Fig. S29. Tauc plots of **L1**, **L2** and **L3** film.

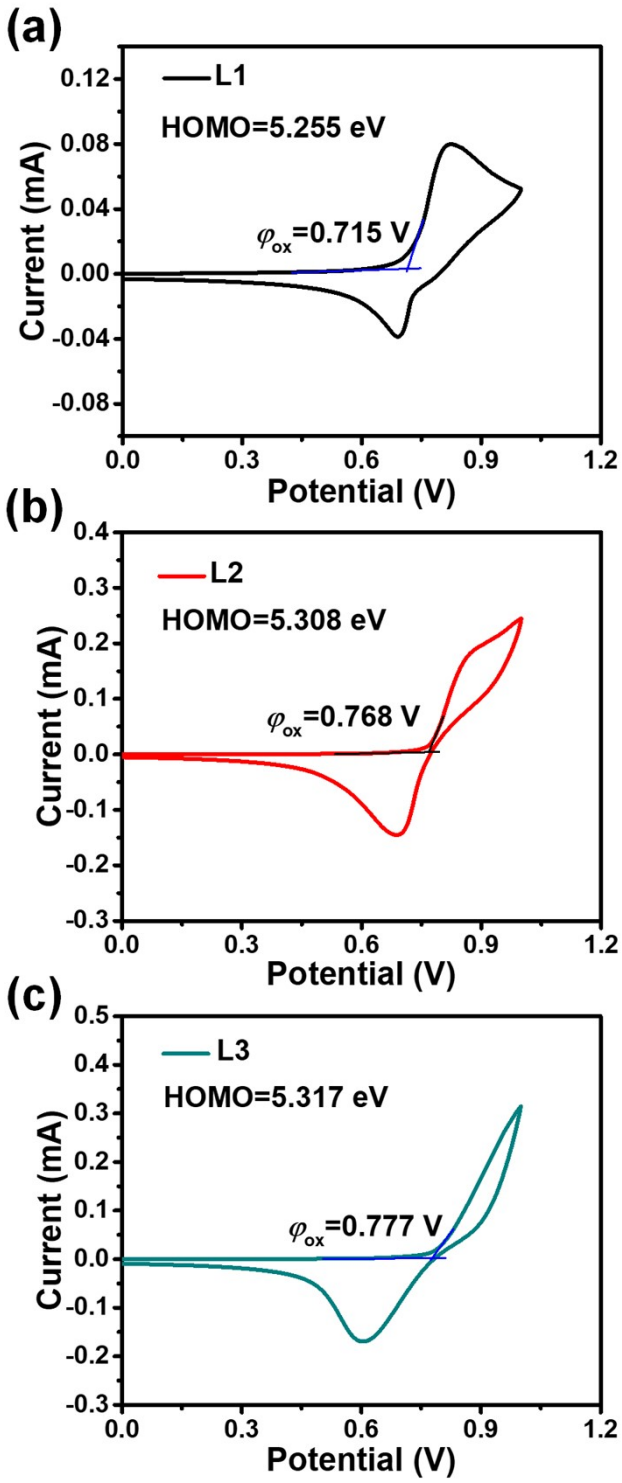

Fig. S30. Cyclic voltammograms of (a) **L1**, (b) **L2** and (c) **L3** film. With the saturated calomel electrode (SCE) as the reference electrode, the energy level of the molecules was calculated according to the equation: E_{HOMO}=-(4.8+E_{ox}-E_f) (eV), where E_{ox} is the initial oxidation potential, E_f is 0.26. The calculated HOMO levels of **L1**, **L2** and **L3** are -5.255, -5.308 and -5.317 eV, respectively.

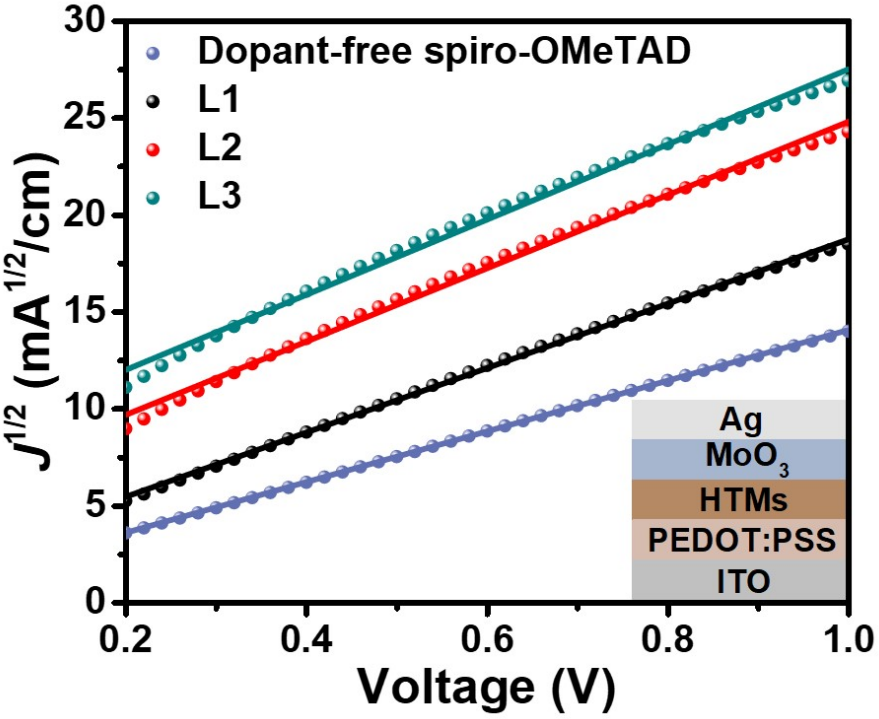

Fig. S31. *J-V* curves of hole-only ITO/PEDOT:PSS/HTM/MoO_3/Ag devices.

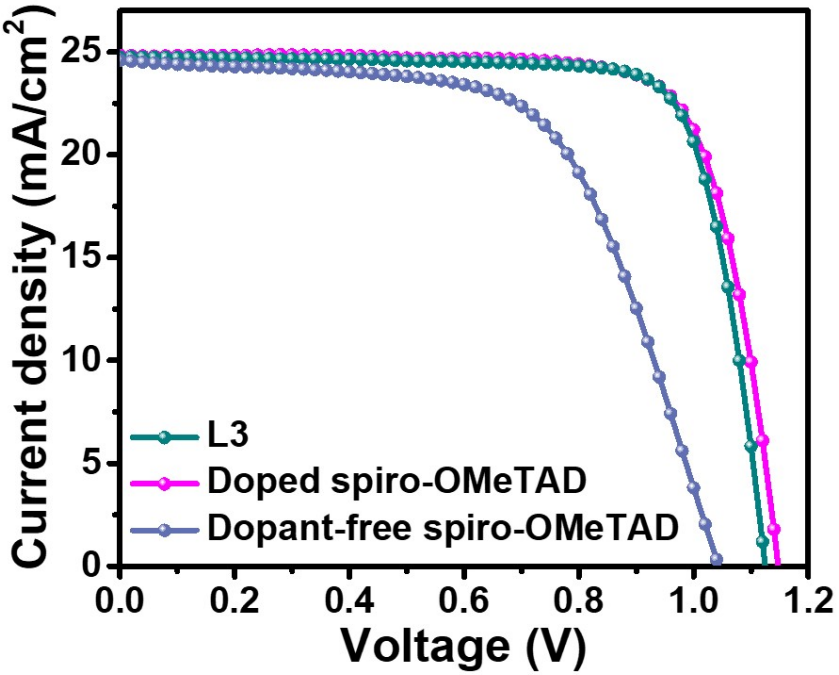

Fig. S32. *J-V* curves of PSCs with doped **spiro-OMeTAD**, dopant-free **spiro-OMeTAD** and **L3** HTM.

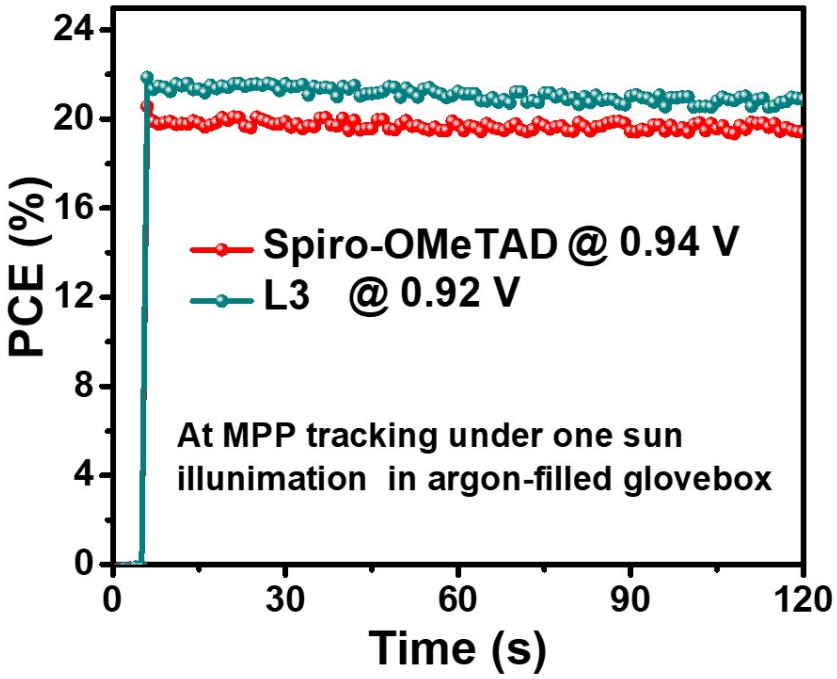

Fig. S33. Stable power output of the best devices with doped **spiro-OMeTAD** and dopant-free **L3** HTL.

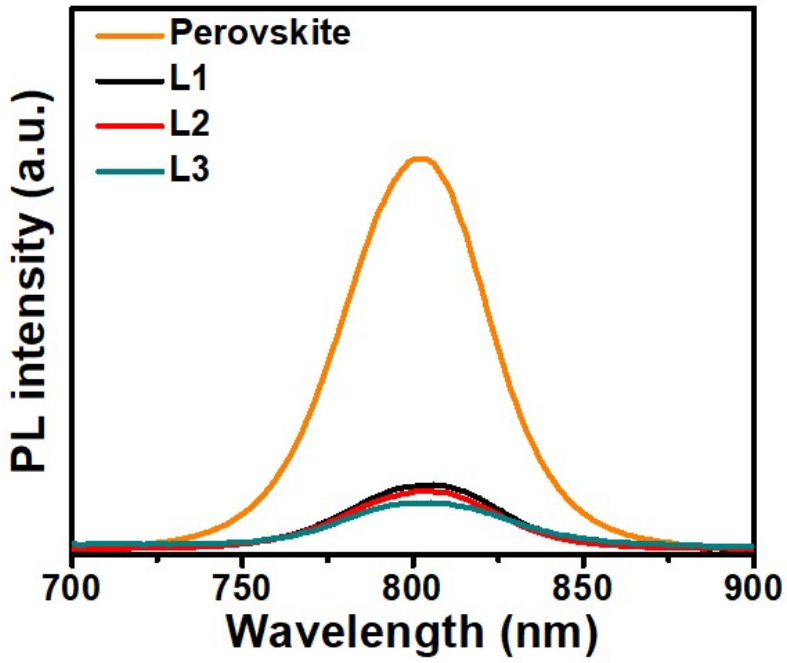

Fig. S34. Steady-state PL of perovskite film and perovskite film covered with **L1**, **L2** and **L3**, respectively.

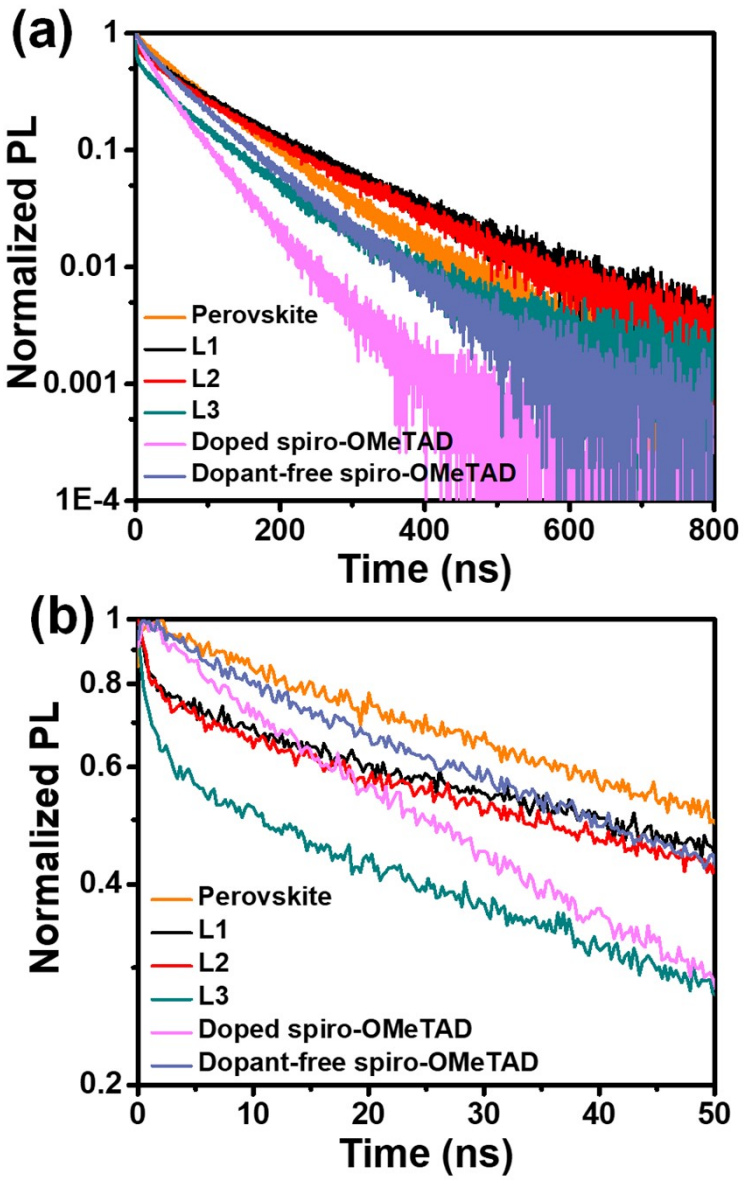

Fig. S35. (a) Time-resolved PL of the perovskite film cover with doped **spiro-OMeTAD**, dopant-free **spiro-OMeTAD** and **L1-3** HTM. (b) Zoom-in to Fig. S36a.

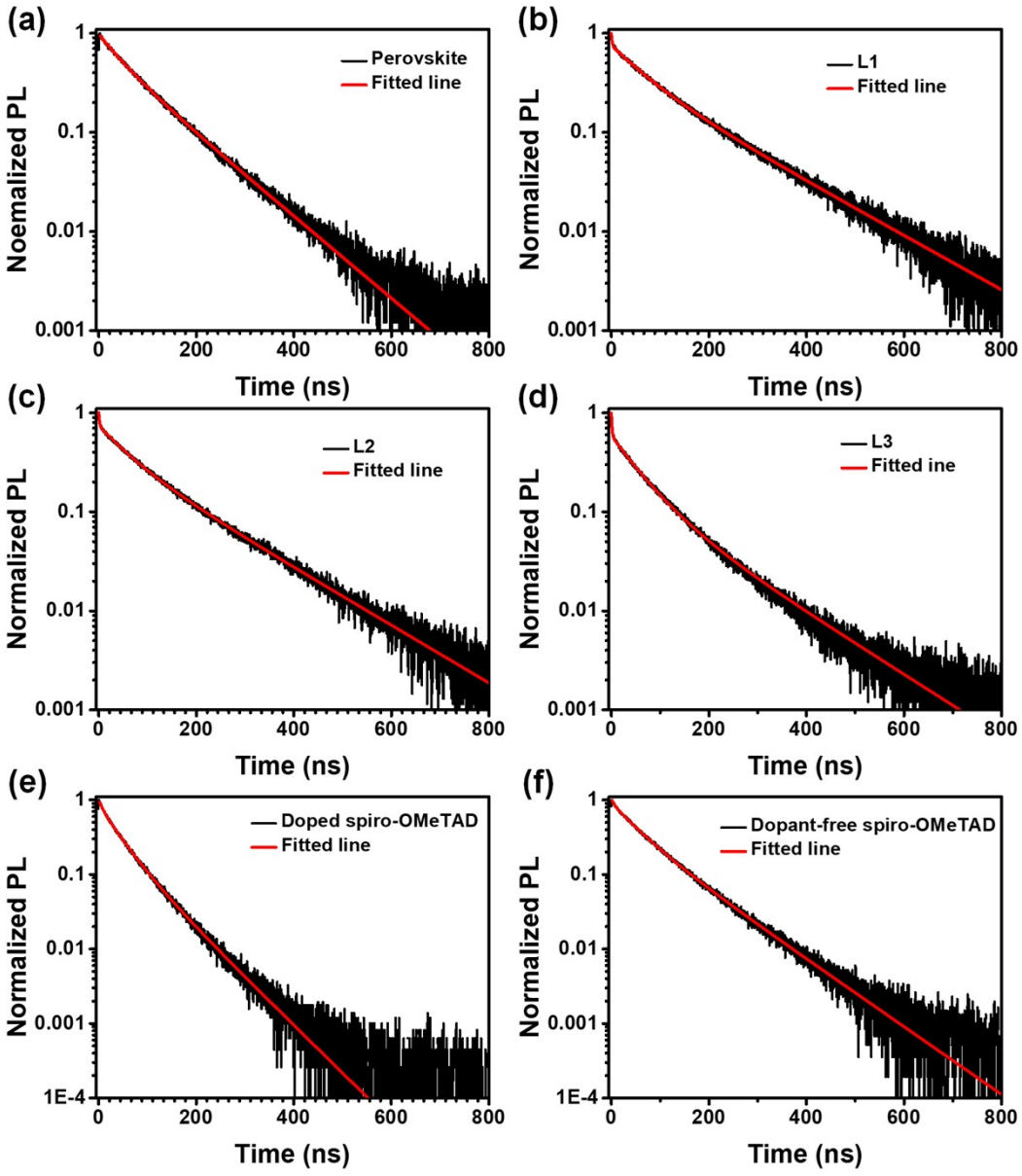

Fig. S36. (a) Time-resolved PL of the perovskite film cover with doped **spiro-OMeTAD**, dopant-free **spiro-OMeTAD** and **L1-3** HTM. (a) bare perovskite film, (b) perovskite film with **L1** HTM, (c) perovskite film with **L2** HTM, (d) perovskite film with **L3** HTM, (e) perovskite film with doped **spiro-OMeTAD** HTM, (f) perovskite film with dopant-free **spiro-OMeTAD** HTM. The corresponding TRPL curves were a good fit by multiple exponential functions to help with the differential lifetime evaluations. For the pure perovskite in (a), a bi-exponential fitting gave a good convergence. The two components of intermediate and long lifetimes, summarized in Table S6, is due to recombination at the surface/grain boundaries, and the intrinsic PL

lifetime of the bulk perovskite. For (b-f), triple-exponential functions gave better convergences (not based on an explicit physical model), which includes a fast component (lifetime τ_1, and weight fraction A_1), an intermediate component (lifetime τ_2, and weight fraction A_2), and a slow component (lifetime τ_3, and weight fraction A_3). The fast component in the samples with HTMs, mainly corresponds to the rapid quenching process of photogeneration of free carriers of perovskite through charge extraction from the perovskite to the HTMs. The overall decay time remains long in the L-series samples due to an increased τ_2 and τ_3, which we attribute to passivation of the perovskite by the functional group. [Sol. RRL 2022, 6, 2200224] Passivation can give rise to significant increases in the decay lifetime that is reflected in the τ_2 and τ_3 parameters in the L-series HTLs.

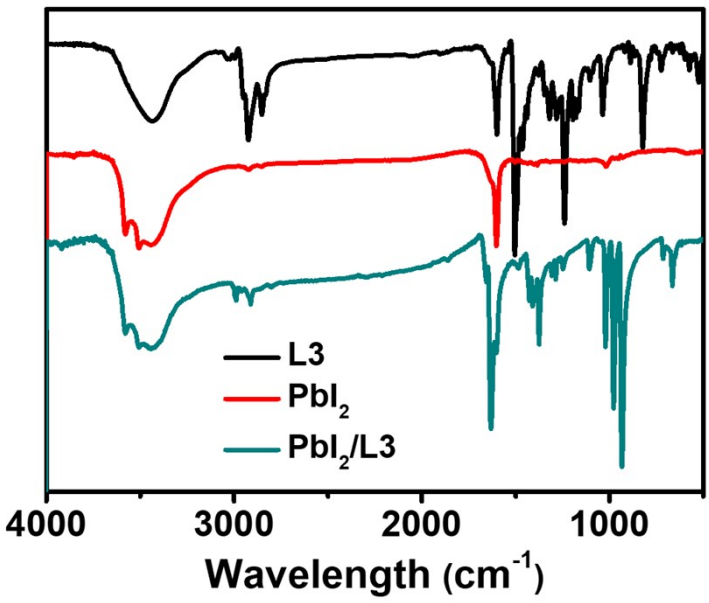

Fig. S37 Full FTIR spectra of the powders of L3, PbI_2 and PbI_2/L3 blend. The PbI_2/L3 sample was mixed PbI_2 solution and L3 solution directly, then the powder was dried at 80 °C for eight hours.

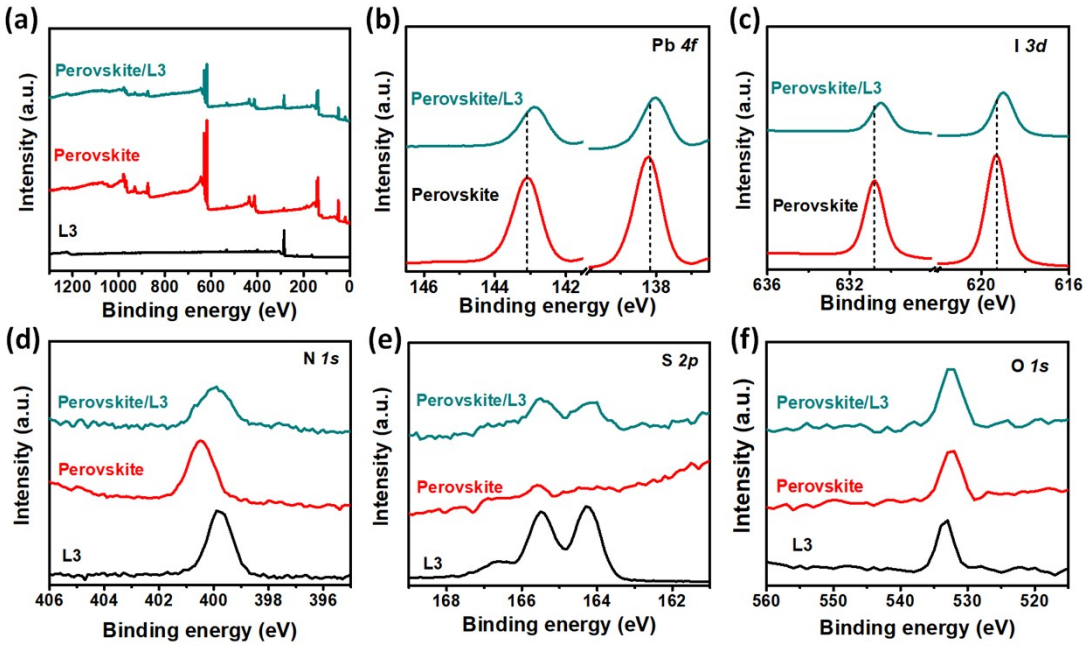

Fig. S38 The XPS spectrum of the perovskite film, L3 film, and perovskite/L3 film. (a) full spectrum, (b) Pb 4f, (c) I 3d (d) N 1s (e) S 2p and (f) O 1s.

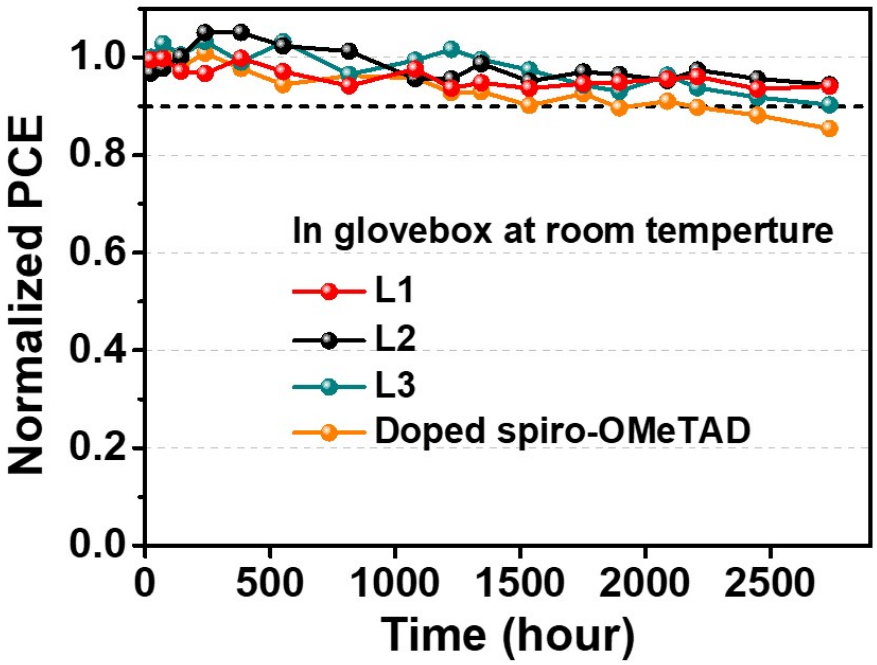

Fig. S39 Long-term stability of unencapsulated control PSC (doped spiro-OMeTAD) and dopant-free L-series PSC stored at argon-filled glovebox.

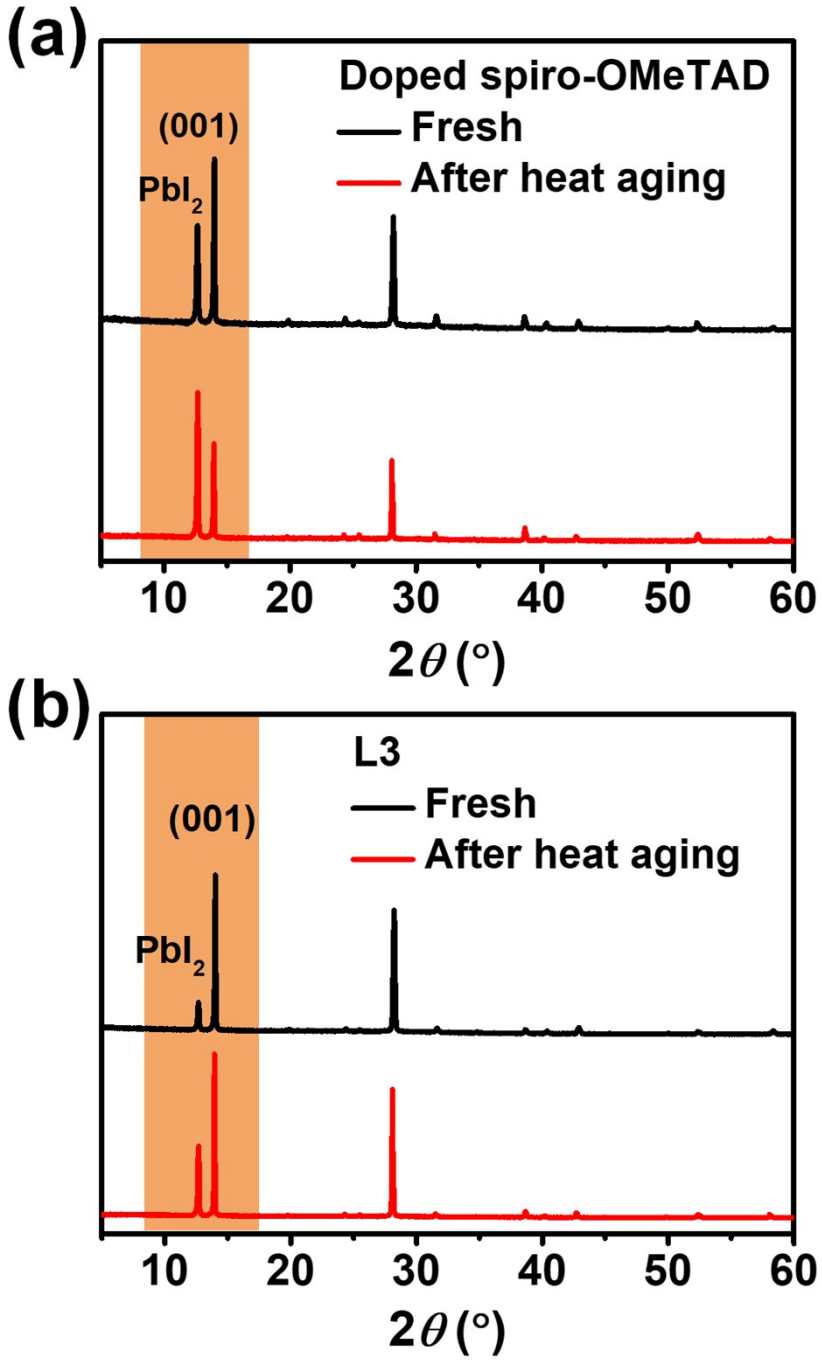

Fig. S40 XRD patterns for doped spiro-OMeTAD perovskite film and L3-perovskite film before and after 85°C aging for 10 days in the argon.

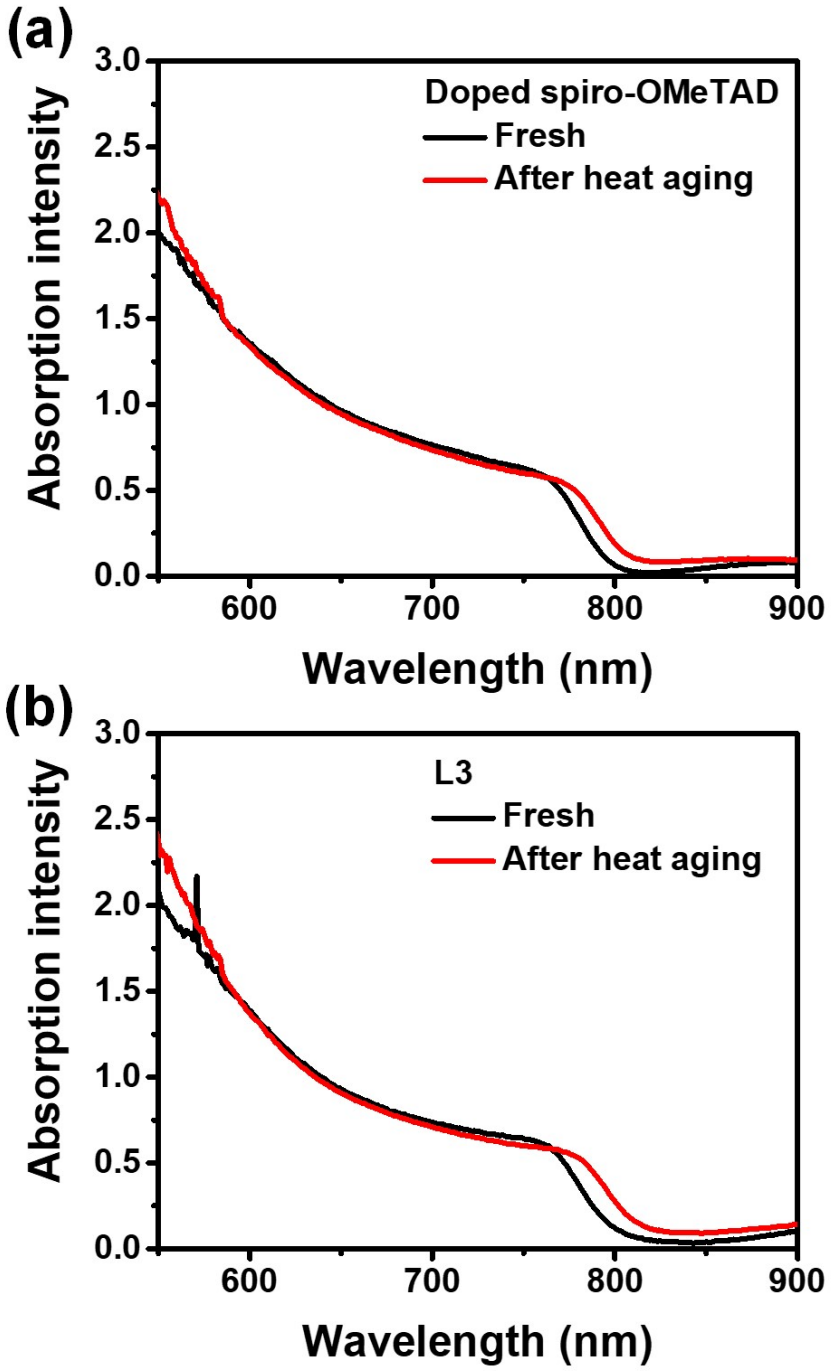

Fig. S41 The absorption spectra of perovskite film coved with doped spiro-OMeTAD and L3 HTL before and after 85°C aging for 10 days in the argon. (a) doped spiro-OMeTAD HTL, (b) L3 HTL.

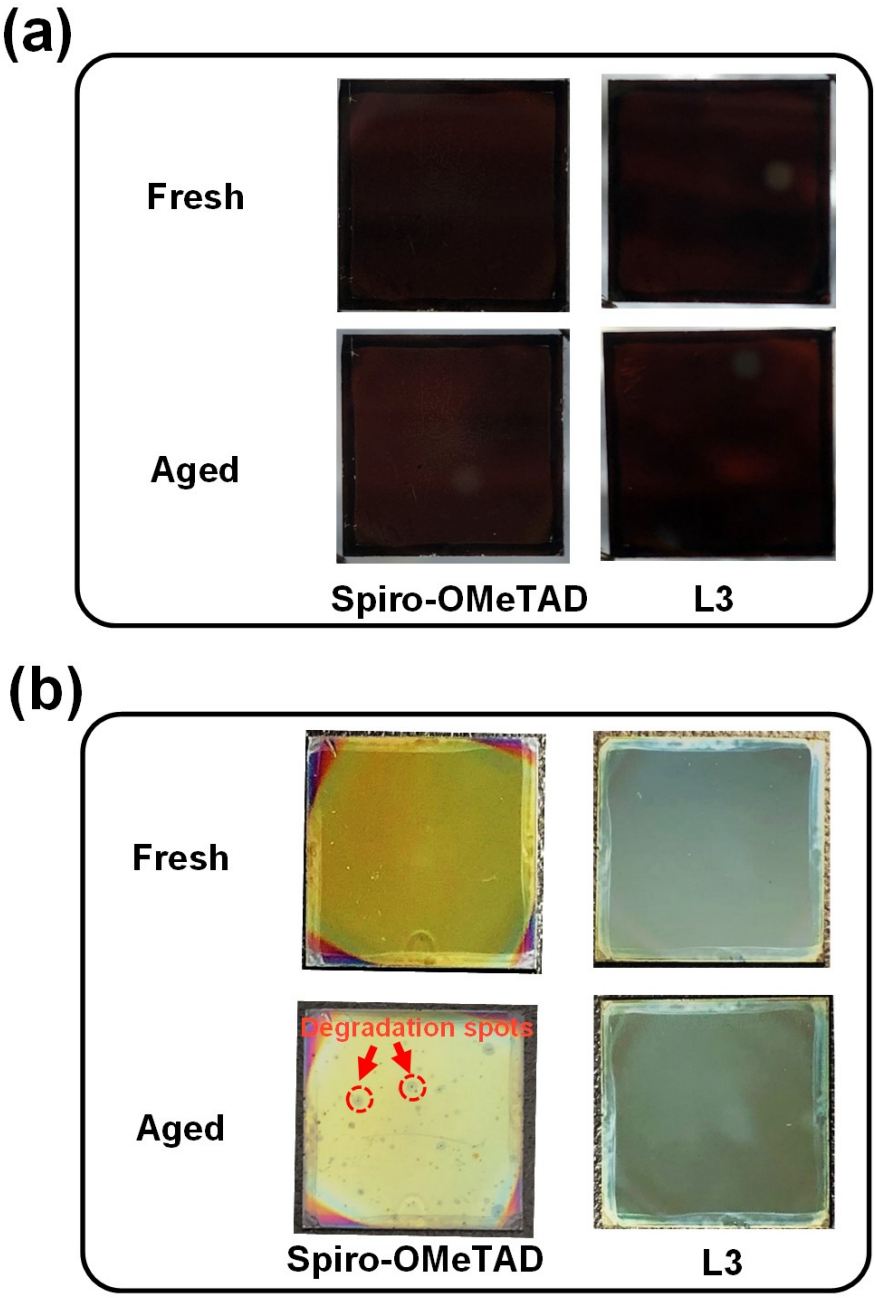

Fig. S42. Photo images for perovskite film with doped spiro-OMeTAD HTL and L3 HTL before and after 85°C aging for 10 days in the argon. (a) glass side, (b) top side.

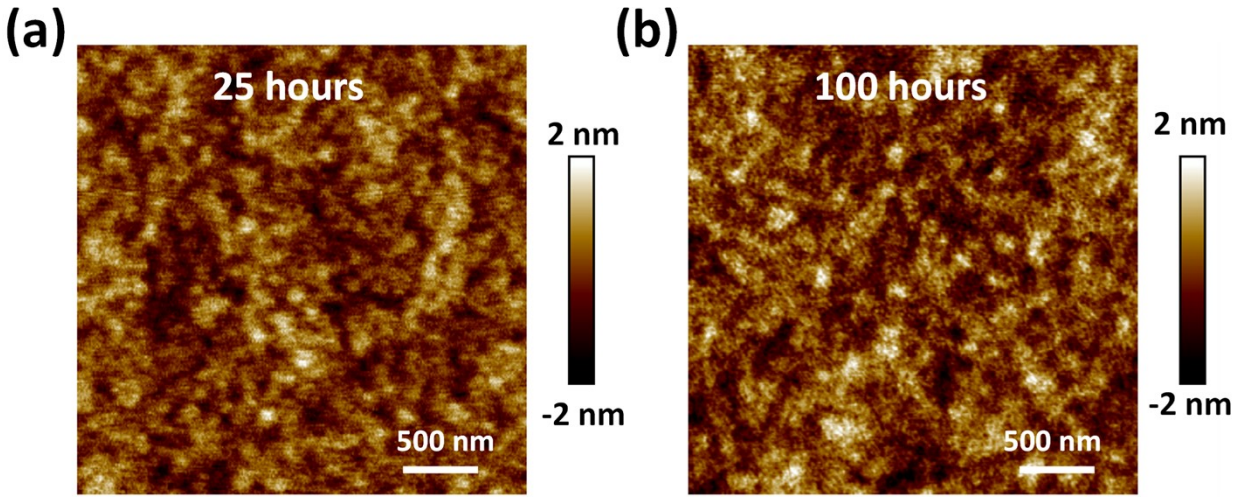

Fig. S43 AFM images of L3 HTMs on ITO substrates, the aging condition is 100°C for (a) 25 hours and (b) 100 hours on the hotplate in N_2-filled glovebox.

Table S1. Summary of thermal stability (at 85°C or MPP tracking at over 70°C) of the state-of-the-art p-i-n and n-i-p PSCs.

Journal	Structure	Stability	Ref.
p-i-n PSCs			
Science	FTO/poly-TPD/$Cs_{0.17}FA_{0.83}Pb(I_{1-X}Br_X)_3$/PCBM/BCP/Cr/Cu	Under full-spectrum sunlight **at 85°C** in ambient air, encapsulated, T_{95}=1200 h.	13
Nat. Energy	ITO/PTAA/perovskite/C_{60}/BCP/Cu	**T=85°C**, T_{90}=1020 h	14
Science	ITO/P3CT-N/$(FAPbI_3)_{0.95}(MAPbBr_3)_{0.05}$/PCBM/$C_{60}$/TPBi/Cu	**T=85°C,** maintained 91.8% for >2200 h.	15
Energy Environ. Sci.	ITO/p-PY/perovskite/PCBM/BCP/Ag	**T=85°C**, maintained over 94% for 500 h, **T=120°C,** maintained over 81% for 200 h.	16
Science	ITO/PTAA/perovskite/C_{60}/BCP/Ag	**Damp heat test (85°C/85%)**, T_{95}>1000 h,	17
Science	ITO/2PACz/3D-perovskite/2D-perovskite/C_{60}/BCP/Ag	**Damp heat test (85°C/85%)**, T_{95}>1200 h.	18
Nature	FTO/NiO/perovskite/PCBM/BCP/Cr/Cr_2O_3/Au	Full spectrum sunlight at **70 to 75°C,** encapsulated, T_{95}=1800 h.	19
n-i-p PSCs			
Joule	FTO/TiO_2/ZrO_2/5AVA$_X$MAPbI$_{1-3}$/carbon	**Damp heat test (85°C/85%**), 1100 h without decay; T=55°C, 9,000 h operational tracking without obvious decay	20
Nat. Energy	FTO/SnO_2/3D:SIG-2D/P3HT/Au	**Damp heat test (85°C/85%),** T_{95}=1056 h	21
Science	ITO/c-TiO_2/TiO_2 nanorods/PMMA:PCBM/ $Cs_{0.05}FA_{0.88}MA_{0.07}PbI_{2.56}Br_{0.44}$/PMMA/P3HT:CuPc/Au	**Damp heat test (85°C/85%)**, retained ~95.3% of for >260 h.	22
Science	ITO/SnO_2/3D Perovskite/2D perovskite /spiro-OMeTAD/Au	**T=85°C**, T_{80}=500 h	23
Science	FTO/compact-TiO_2/ mp-TiO_2/perovskite/Spiro-OMeTAD/Au	**T=85°C**, RH=15-25%, T_{80}=1300 h	24

Table S2. Summary of recent developments of doping-free molecule HTMs in *n-i-p* PSCs.

HTM	Perovskite	V_{oc} (V)	J_{sc} (mA/cm^2)	FF (%)	PCE (%)	*Tg* (°C)	Atmosphere	Thermal stability	Publish data	Ref.
Polymer HTMs										
asy-PBTBDT	$Cs_{0.05}FA_{0.81}MA_{0.14}PbI_{2.55}Br_{0.45}$	1.11	22.4	73.2	**18.3**	/		/	2017.08	25
PTEG	Cs-perovskite	1.14	22.5	77.0	**19.8**	/		/	2017.09	26
P3HT	$(FAPbI_3)_{0.95}(MAPbBr_3)_{0.05}$	1.152	24.88	81.4	**23.3**	/		/	2019.03	27
PTB1-C	CsFAMAGA mixed perovskite	1.05	22.37	81.2	**19.06**	/		/	2019.09	28
P3	$MAPbI_3$	1.11	22.8	80.0	**20.3**	/		/	2019.11	29
PBDTT	Cs-perovskite	1.12	23.64	76.67	**20.28**	/		/	2019.12	30
PBTT-T	CsFAMA mixed perovskite	1.14	21.68	76.79	**19.02**	/		/	2020.11	31
alkoxy-PTEG	$Cs_{0.06}FA_{0.78}MA_{0.16}Pb_{0.94}I_{2.4}Br_{0.48}$	23.2	1.14	79.8	**21.2**	/		/	2020.01	32
PBTFO	$Cs_{0.05}(FA_{0.85}MA_{0.15})_{0.95}Pb(I_{0.85}Br_{0.15})_3$	1.21	23.3	75.1	**22.10**	/	N_2	*T*=65°C, unencapsulated, after 500 hours maintains 97%	2020.01	33
PBDT-N20	$(FAPbI_3)_{0.85}(MAPbBr_3)_{0.15}$	1.08	23.4	75.0	**18.9**	/	Glovebox	*T*=80 °C, after 1500 h maintains over 95%	2020.09	34
PC3	$MAPbI_3$	23.5	1.11	80.0	**20.8**	/	/	*T*=85°C, under 1 sun illumination after 200 h maintains 70%	2020.09	35

PE10	$FA_{0.85}MA_{0.15}PbI_3$	1.16	24.1	79.8	**22.3**			T = 85°C, in dark, after 500 h with 45−85% RH maintains 80.5% *T*=85°C, under 1 sun illumination after 240 h maintains 65%	2022.03	36
Ploy-alloy (PM6/PMSe)	$MA_{0.16}FA_{0.84}PbI_3$	1.19	25.07	82.17	**24.53**		N_2	T = 80 °C, in dark, after 600 h maintains 93%	2022.05	37
PM6	$MA_{0.16}FA_{0.84}PbI_3$	1.19	24.55	82.22	**24.04**			/	2022.08	38
PFBTI	$Cs_{0.05}FA_{0.95}PbI_3$	1.16	24.6	80.8	**23.1**			/	2022.10	39
Small molecule HTMs										
2DP-TDB	$FA_{0.85}MA_{0.15}PbI_3$	1.16	24.02	79.57	**22.17**		N_2	*T*=80°C, unencapsulated, in dark, after 376 h maintains 81%	2021.03	40
Z26	$(FAPbI_3)_{0.85}(MAPbBr_3)_{0.15}$	1.132	23.59	75.0	**20.1**	**98**	40% RH	*T*=65°C, unencapsulated, in dark after 120 h maintains ~85%	2017.09	41
TQ2	$MAPbI_3$	1.12	22.55	77.67	**19.62**	**113**		/	2018.07	42
TTE-2	$(FAPbI_3)_{0.95}(MAPbBr_3)_{0.05}$	1.11	23.26	77.52	**20.04**	**158**		/	2019.01	43
YN3	$(FAPbI_3)_{0.85}(MAPbBr_3)_{0.15}$	1.12	22.43	75	**18.84**	/		/	2019.02	44
DTPC13-ThTPA	$MA_{0.7}FA_{0.3}PbI_{2.85}Br_{0.15}$	1.135	22.82	78.7	**20.38**	/		/	2019.07	4
M129	$Cs_{0.05}(FA_{0.83}MA_{0.17})_{0.95}Pb(Br_{0.17}I_{0.83})_3$	1.08	22.50	72.0	**17.50**	**170**	N_2	*T*=60 °C, after 72 h maintains 90%	2019.09	45
BTTI-C6	CsFAMA perovskite	1.10	24.00	74.6	**19.69**	**224**	N_2	*T*=100 °C, unencapsulated, after 60 h maintains 70%	2019.12	3
DTP-C6Th	$MA_{0.7}FA_{0.3}Pb(I_{0.925}Br_{0.075})_3$	1.157	22.76	79.9	**21.04**	**84.5**		/	2019.07	5
YZ22	$Cs_{0.1}FA_{0.9}PbI_3$	1.10	25.1	81.0	**22.4**	**108**	Air	*T*=85°C, encapsulated, MPP (1.1 sun) tracking after 60 h maintains 60%	2020.09	7
TQ4	$Cs_{0.05}FA_{0.85}MA_{0.1}Pb(I_{0.97}Br_{0.03})_3$	1.124	23.78	79.0	**21.03**	**131**	N_2	*T*=85°C, in dark, after100 h maintains 90%	2020.10	8
DTB-FL	$Cs_{0.05}FA_{0.95}PbI_3$	1.14	23.8	77.4	**21.50**	**87**	N_2	*T*=80°C, after 240 h maintains 68%	2020.12	11
MeOTTVT	$Cs_{0.05}FA_{0.85}MA_{0.10}Pb(I_{0.97}Br_{0.03})_3$	1.11	23.89	80.3	**21.30**	**137.1**	/	*T*=80°C, in dark, after 220 h maintains 90%	2020.12	46
SFDT-TDM	$Cs_xFA_{1-x}PbI_3$	1.13	24.1	79.5	**21.7**	/		/	2021.06	47
CB	$MAPbI_3$	1.15	23.60	77.7	**21.09**			/	2021.08	48
BDT-DPA-F	$FAMAPbI_3$	1.18	24.66	79.57	**23.12**	/		*T*=85°C, in dark, after 1200 h maintains 80.3%	2022.09	12
L3	(Cs/GA) doped $(FAPbI_3)_{0.95}(MAPbBr_3)_{0.05}$	1.12	25.25	79.84	**22.61**	**163**	**Argon**	***T*=85°C, in dark, after 1000 h maintains 83%** ***T*=85°C, MPP tracking after 500 h maintains >85%**	/	This work

Table S3. Summary of device performance of PSCs with L3 HTL fabricated by different concentration at a speed 4000 rpm. The thicknesses of L3 film on ITO glass were determined using by using a Profilometer (Ambios Tech. XP-2).

Concentration	Thickness (nm)	V_{OC} (V)	J_{SC} (mA/cm²)	FF (%)	PCE (%)
7.5 mg/mL	~33	1.06	21.22	58.77	13.25
10 mg/mL	~45	1.10	24.08	70.02	18.63
12 mg/mL	~54	1.10	24.65	78.15	21.15
15 mg/mL	~61	1.10	24.62	75.87	20.49

Table S4. Summary of device performance of PSCs with L3 HTL fabricated by different speed of spin-coating with a precursor of 12 mg/mL in CB.

12 mg/mL L3 HTL	V_{OC} (V)	J_{SC} (mA/cm^2)	FF (%)	PCE (%)
2K	1.11	23.91	72.11	19.06
4K	1.11	24.48	76.33	20.78
6K	1.11	24.22	76.45	20.57

Table S5. Summary of the performance of PSCs with different HTMs.

HTL	V_{OC} (V)	J_{SC} (mA/cm^2)	FF (%)	PCE (%)
L1	1.08 ± 0.01	24.41± 0.41	69.53 ± 2.61	18.39 ± 0.81
L2	1.10 ± 0.01	24.66 ± 0.32	74.89 ± 1.08	20.37 ± 0.36
L3	1.11 ± 0.01	24.77 ± 0.27	76.42 ± 1.60	21.11 ± 0.49

Table S6. Lifetimes and weighted fractions fitted by triple-exponential functions from the TRPL.

	A_1	τ_1 (ns)	A_2	τ_2 (ns)	A_3	τ_3 (ns)	τ_{avg} (ns)
Pristine			0.34	44.51	0.66	104.91	84.4
L1	0.22	1.60	0.37	63.48	0.41	158.89	88.98
L2	0.24	1.60	0.34	56.55	0.42	149.00	82.2
L3	0.37	1.39	0.45	53.95	0.18	138.81	49.8
Dopant-free spiro-OMeTAD	0.13	5.66	0.41	46.26	0.46	95.60	63.7
Doped spiro-OMeTAD	0.16	6.59	0.50	34.48	0.34	67.56	41.3

$$\tau_{avg} = \frac{\sum A_i \tau_i}{\sum A_i}$$

Reference

1. M. Jeong, W. Choi In, M. Go Eun, Y. Cho, M. Kim, B. Lee, S. Jeong, Y. Jo, W. Choi Hye, J. Lee, J.-H. Bae, K. Kwak Sang, S. Kim Dong and C. Yang, *Science*, 2020, **369**, 1615-1620.
2. Y. Liu, Q. Chen, H.-S. Duan, H. Zhou, Y. Yang, H. Chen, S. Luo, T.-B. Song, L. Dou, Z. Hong and Y. Yang, *J. Mater. Chem. A*, 2015, **3**, 11940-11947.
3. B. Tu, Y. Wang, W. Chen, B. Liu, X. Feng, Y. Zhu, K. Yang, Z. Zhang, Y. Shi, X. Guo, H. F. Li, Z. Tang, A. B. Djurisic and Z. He, *ACS Appl. Mater. Interfaces*, 2019, **11**, 48556-48563.
4. J. Zhou, X. Yin, Z. Dong, A. Ali, Z. Song, N. Shrestha, S. S. Bista, Q. Bao, R. J. Ellingson, Y. Yan and W. Tang, *Angew. Chem. Int. Ed.*, 2019, **58**, 13717-13721.
5. X. Yin, J. Zhou, Z. Song, Z. Dong, Q. Bao, N. Shrestha, S. S. Bista, R. J. Ellingson, Y. Yan and W. Tang, *Adv. Funct. Mater.*, 2019, **29**, 1904300.
6. Y. Liu, Z. Hong, Q. Chen, H. Chen, W.-H. Chang, Y. Yang, T.-B. Song and Y. Yang, *Adv. Mater.*, 2016, **28**, 440-446.
7. B. X. M. Zhao, C. Yao, K. C. Gu, T. R. Liu, Y. Xia and Y. L. Loo, *Energy Environ. Sci.*, 2020, **13**, 4334-4343.
8. H. Guo, H. Zhang, C. Shen, D. Zhang, S. Liu, Y. Wu and W. H. Zhu, *Angew. Chem. Int. Ed.*, 2021, **60**, 2674-2679.
9. M. Cheng, K. Aitola, C. Chen, F. Zhang, P. Liu, K. Sveinbjörnsson, Y. Hua, L. Kloo, G. Boschloo and L. Sun, *Nano Energy*, 2016, **30**, 387-397.
10. P. Xu, P. Liu, Y. Li, B. Xu, L. Kloo, L. Sun and Y. Hua, *ACS Appl. Mater. Interfaces*, 2018, **10**, 19697-19703.
11. T. Niu, W. Zhu, Y. Zhang, Q. Xue, X. Jiao, Z. Wang, Y.-M. Xie, P. Li, R. Chen, F. Huang, Y. Li, H.-L. Yip and Y. Cao, *Joule*, 2021, **5**, 249-269.
12. Q. Cheng, H. Chen, F. Yang, Z. Chen, W. Chen, H. Yang, Y. Shen, X. M. Ou, Y. Wu, Y. Li and Y. Li, *Angew. Chem. Int. Ed.*, 2022, **61**, e202210613.
13. Y.-H. Lin, N. Sakai, P. Da, J. Wu, H. C. Sansom, A. J. Ramadan, S. Mahesh, J. Liu, R. D. J. Oliver, J. Lim, L. Aspitarte, K. Sharma, P. K. Madhu, A. B. Morales-Vilches, P. K. Nayak, S. Bai, F. Gao, C. R. M. Grovenor, M. B. Johnston, J. G. Labram, J. R. Durrant, J. M. Ball, B. Wenger, B. Stannowski and H. J. Snaith, *Science*, 2020, **369**, 96.
14. X. Zheng, Y. Hou, C. Bao, J. Yin, F. Yuan, Z. Huang, K. Song, J. Liu, J. Troughton, N. Gasparini, C. Zhou, Y. Lin, D.-J. Xue, B. Chen, A. K. Johnston, N. Wei, M. N. Hedhili, M. Wei, A. Y. Alsalloum, P. Maity, B. Turedi, C. Yang, D. Baran, T. D. Anthopoulos, Y. Han, Z.-H. Lu, O. F. Mohammed, F. Gao, E. H. Sargent and O. M. Bakr, *Nat. Energy*, 2020, **5**, 131-140.
15. X. Li, W. Zhang, X. Guo, C. Lu, J. Wei and J. Fang, *Science*, 2022, **375**, 434-437.
16. R. Chen, S. Liu, X. Xu, F. Ren, J. Zhou, X. Tian, Z. Yang, X. Guanz, Z. Liu, S. Zhang, Y. Zhang, Y. Wu, L. Han, Y. Qi and W. Chen, *Energy Environ. Sci.*, 2022, **15**, 2567-2580.
17. Z. Li, B. Li, X. Wu, A. Sheppard Stephanie, S. Zhang, D. Gao, J. Long Nicholas and Z. Zhu, *Science*, 2022, **376**, 416-420.
18. R. Azmi, E. Ugur, A. Seitkhan, F. Aljamaan, A. S. Subbiah, J. Liu, G. T.

Harrison, M. I. Nugraha, M. K. Eswaran, M. Babics, Y. Chen, F. Xu, T. G. Allen, A. U. Rehman, C. L. Wang, T. D. Anthopoulos, U. Schwingenschlogl, M. De Bastiani, E. Aydin and S. De Wolf, *Science*, 2022, **376**, 73-77.
19. S. Bai, P. Da, C. Li, Z. Wang, Z. Yuan, F. Fu, M. Kawecki, X. Liu, N. Sakai, J. T.-W. Wang, S. Huettner, S. Buecheler, M. Fahlman, F. Gao and H. J. Snaith, *Nature*, 2019, **571**, 245-250.
20. A. Mei, Y. Sheng, Y. Ming, Y. Hu, Y. Rong, W. Zhang, S. Luo, G. Na, C. Tian, X. Hou, Y. Xiong, Z. Zhang, S. Liu, S. Uchida, T.-W. Kim, Y. Yuan, L. Zhang, Y. Zhou and H. Han, *Joule*, 2020, **4**, 2646-2660.
21. Y.-W. Jang, S. Lee, K. M. Yeom, K. Jeong, K. Choi, M. Choi and J. H. Noh, *Nat. Energy*, 2021, **6**, 63-71.
22. J. Peng, D. Walter, Y. Ren, M. Tebyetekerwa, Y. Wu, T. Duong, Q. Lin, J. Li, T. Lu, M. A. Mahmud, O. L. C. Lem, S. Zhao, W. Liu, Y. Liu, H. Shen, L. Li, F. Kremer, H. T. Nguyen, D.-Y. Choi, K. J. Weber, K. R. Catchpole and T. P. White, *Science*, 2021, **371**, 390.
23. T. Bu, J. Li, H. Li, C. Tian, J. Su, G. Tong, L. K. Ono, C. Wang, Z. Lin, N. Chai, X.-L. Zhang, J. Chang, J. Lu, J. Zhong, W. Huang, Y. Qi, Y.-B. Cheng and F. Huang, *Science*, 2021, **372**, 1327.
24. G. Kim, H. Min, K. S. Lee, D. Y. Lee, S. M. Yoon and S. I. Seok, *Science*, 2020, **370**, 108-112.
25. J. Lee, M. Malekshahi Byranvand, G. Kang, S. Y. Son, S. Song, G. W. Kim and T. Park, *J. Am. Chem. Soc.*, 2017, **139**, 12175-12181.
26. G.-W. Kim, J. Lee, G. Kang, T. Kim and T. Park, *Adv. Energy Mater.*, 2018, **8**, 1701935.
27. E. H. Jung, N. J. Jeon, E. Y. Park, C. S. Moon, T. J. Shin, T. Y. Yang, J. H. Noh and J. Seo, *Nature*, 2019, **567**, 511-515.
28. F. Qi, X. Deng, X. Wu, L. J. Huo, Y. Q. Xiao, X. H. Lu, Z. L. Zhu and A. K. Y. Jen, *Adv. Energy Mater.*, 2019, **9**, 1902600.
29. F. Zhang, Z. Yao, Y. Guo, Y. Li, J. Bergstrand, C. J. Brett, B. Cai, A. Hajian, Y. Guo, X. Yang, J. M. Gardner, J. Widengren, S. V. Roth, L. Kloo and L. Sun, *J. Am. Chem. Soc.*, 2019, **141**, 19700-19707.
30. G. You, Q. Zhuang, L. Wang, X. Lin, D. Zou, Z. Lin, H. Zhen, W. Zhuang and Q. Ling, *Adva. Energy Mater.*, 2019, **10**, 1903146.
31. L. Wang, Q. Zhuang, G. You, X. Lin, K. Li, Z. Lin, H. Zhen and Q. Ling, *ACS Appl. Energy Mater.*, 2020, **3**, 12475-12483.
32. J. Lee, G. W. Kim, M. Kim, S. A. Park and T. Park, *Adv. Energy Mater.*, 2020, **10**, 1902662.
33. Z. J. Li, J. Park, H. Park, J. Lee, Y. Kang, T. K. Ahn, B. G. Kim and H. J. Park, *Nano Energy*, 2020, **78**, 105159.
34. X. Q. Jiang, X. Liu, J. F. Zhang, S. Ahmad, D. D. Tu, W. Qin, T. G. Jiu, S. P. Pang, X. Guo and C. Li, *J. Mater. Chem. A*, 2020, **8**, 21036-21043.
35. Z. Yao, F. Zhang, Y. Guo, H. Wu, L. He, Z. Liu, B. Cai, Y. Guo, C. J. Brett, Y. Li, C. V. Srambickal, X. Yang, G. Chen, J. Widengren, D. Liu, J. M. Gardner, L. Kloo and L. Sun, *J. Am. Chem. Soc.*, 2020, **142**, 17681-17692.

36. Z. Yao, F. Zhang, L. He, X. Bi, Y. Guo, Y. Guo, L. Wang, X. Wan, Y. Chen and L. Sun, *Angew. Chem. Int. Ed.*, 2022, **61**, e202201847.
37. Q. Fu, X. Tang, H. Liu, R. Wang, T. Liu, Z. Wu, H. Y. Woo, T. Zhou, X. Wan, Y. Chen and Y. Liu, *J. Am. Chem. Soc.*, 2022, **144**, 9500-9509.
38. Q. Fu, H. Liu, S. Li, T. Zhou, M. Chen, Y. Yang, J. Wang, R. Wang, Y. Chen and Y. Liu, *Angew. Chem. Int. Ed.*, 2022, **n/a**, e202210356.
39. Y. Bai, Z. Zhou, Q. Xue, C. Liu, N. Li, H. Tang, J. Zhang, X. Xia, J. Zhang, X. Lu, C. J. Brabec and F. Huang, *Adv. Mater.*, 2022, 2110587.
40. Q. Fu, Z. Y. Xu, X. C. Tang, T. T. Liu, X. Y. Dong, X. D. Zhang, N. Zheng, Z. Q. Xie and Y. S. Liu, *Acs Energy Lett.*, 2021, **6**, 1521-1532.
41. F. Zhang, Z. Q. Wang, H. W. Zhu, N. Pellet, J. S. Luo, C. Y. Yi, X. C. Liu, H. L. Liu, S. R. Wang, X. G. Li, Y. Xiao, S. M. Zakeeruddin, D. Q. Bi and M. Gratzel, *Nano Energy*, 2017, **41**, 469-475.
42. H. Zhang, Y. Wu, W. Zhang, E. Li, C. Shen, H. Jiang, H. Tian and W.-H. Zhu, *Chem. Sci.*, 2018, **9**, 5919-5928.
43. C. Shen, Y. Wu, H. Zhang, E. Li, W. Zhang, X. Xu, W. Wu, H. Tian and W. H. Zhu, *Angew. Chem. Int. Ed.*, 2019, **58**, 3784-3789.
44. D. Zhang, P. Xu, T. Wu, Y. Ou, X. Yang, A. Sun, B. Cui, H. Sun and Y. Hua, *J. Mater. Chem. A*, 2019, **7**, 5221-5226.
45. J. Wang, H. Zhang, B. Wu, Z. Wang, Z. Sun, S. Xue, Y. Wu, A. Hagfeldt and M. Liang, *Angew. Chem. Int. Ed.*, 2019, **58**, 15721-15725.
46. H. Zhu, Z. Shen, L. Pan, J. Han, F. T. Eickemeyer, Y. Ren, X. Li, S. Wang, H. Liu, X. Dong, S. M. Zakeeruddin, A. Hagfeldt, Y. Liu and M. Grätzel, *ACS Energy Lett.*, 2020, **6**, 208-215.
47. J. Wang, X. Wu, Y. Z. Liu, T. Qin, K. C. Zhang, N. Li, J. Zhao, R. Q. Ye, Z. X. Fan, Z. G. Chi and Z. L. Zhu, *Adva. Energy Mater.*, 2021, **11**, 2100967.
48. K.-M. Lee, W.-H. Chiu, Y.-H. Tsai, C.-S. Wang, Y.-T. Tao and Y.-D. Lin, *Chem. Eng. J.*, 2022, **427**, 131609.